AD-A135 913 ANALYSIS OF THE KINEMATIC PROPERTIES DATA OF THE SHOULDER COMPLEX DURING..(U OHIO STATE UNIV COLUMBUS DEPT OF ENGINEERING MECHANICS A E ENGIN AUG 83 1/1

UNCLASSIFIED AFAMRL-TR-83-067 F33615-81-C-0500 F/G 6/2 NL

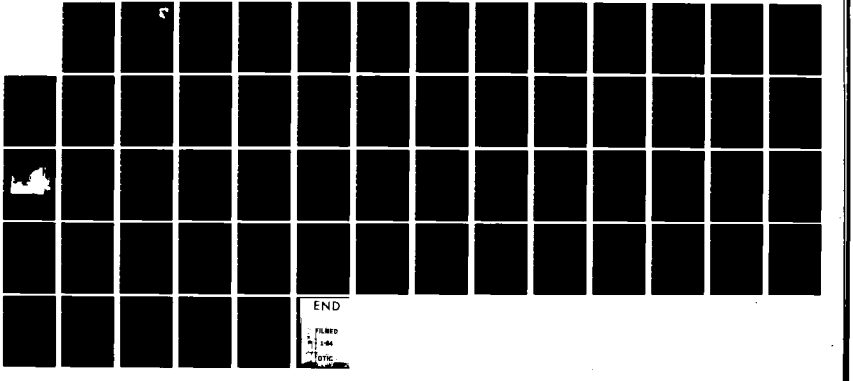

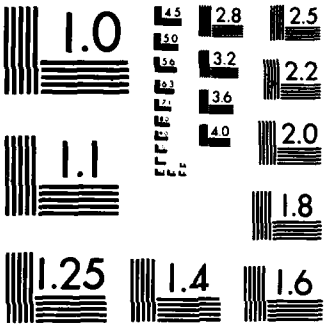

AFAMRL-TR-83-067

ANALYSIS OF THE KINEMATIC PROPERTIES DATA OF THE SHOULDER COMPLEX DURING FORCED MOTION

ALI ERKAN ENGIN

THE OHIO STATE UNIVERSITY
COLUMBUS, OHIO 43210

AUGUST 1983

AIR FORCE AEROSPACE MEDICAL RESEARCH LABORATORY
BIODYNAMICS AND BIOENGINEERING DIVISION
AIR FORCE SYSTEM COMMAND
WRIGHT-PATTERSON AIR FORCE BASE, OHIO 45433

NOTICES

When US Government drawings, specifications, or other data are used for any purpose other than a definitely related Government procurement operation, the Government thereby incurs no responsibility nor any obligation whatsoever, and the fact that the Government may have formulated, furnished, or in any way supplied the said drawings, specifications, or other data, is not to be regarded by implication or otherwise, as in any manner licensing the holder or any other person or corporation, or conveying any rights or permission to manufacture, use, or sell any patented invention that may in any way be related thereto.

Please do not request copies of this report from Air Force Aerospace Medical Research Laboratory. Additional copies may be purchased from:

National Technical Information Service
5285 Port Royal Road
Springfield, Virginia 22161

Federal Government agencies and their contractors registered with Defense Technical Information Center should direct requests for copies of this report to:

Defense Technical Information Center
Cameron Station
Alexandria, Virginia 22314

TECHNICAL REVIEW AND APPROVAL

AFAMRL-TR-83-067

The voluntary informed consent of the subjects used in this research was obtained as required by Air Force Regulation 169-3.

This report has been reviewed by the Office of Public Affairs (PA) and is releasable to the National Technical Information Service (NTIS). At NTIS, it will be available to the general public, including foreign nations.

This technical report has been reviewed and is approved for publication.

FOR THE COMMANDER

Henning E. von Gierke

HENNING E. VON GIERKE, Dr Ing
Director
Biodynamics and Bioengineering Division
Air Force Aerospace Medical Research Laboratory

SECURITY CLASSIFICATION OF THIS PAGE (When Data Entered)

REPORT DOCUMENTATION PAGE

READ INSTRUCTIONS BEFORE COMPLETING FORM

1. REPORT NUMBER: AFAMRL-TR-83-067	2. GOVT ACCESSION NO.: AD-A135913
3. RECIPIENT'S CATALOG NUMBER:	
4. TITLE (and Subtitle): ANALYSIS OF THE KINEMATIC PROPERTIES DATA OF THE SHOULDER COMPLEX DURING FORCED MOTION	5. TYPE OF REPORT & PERIOD COVERED: FINAL REPORT 1 January 1982-31 July 1982
	6. PERFORMING ORG. REPORT NUMBER:
7. AUTHOR(s): Ali Erkan Engin	8. CONTRACT OR GRANT NUMBER(s): F33615-81-C-0500
9. PERFORMING ORGANIZATION NAME AND ADDRESS: Department of Engineering Mechanics, The Ohio State University, Columbus, Ohio 43210	10. PROGRAM ELEMENT, PROJECT, TASK AREA & WORK UNIT NUMBERS: 62202F; 7231-00-01
11. CONTROLLING OFFICE NAME AND ADDRESS: Air Force Aerospace Medical Research Laboratory, Aerospace Medical Div., Air Force Systems Command, Wright-Patterson Air Force Base, Ohio 45433	12. REPORT DATE: August 1983
	13. NUMBER OF PAGES: 59
14. MONITORING AGENCY NAME & ADDRESS (if different from Controlling Office)	15. SECURITY CLASS. (of this report): UNCLASSIFIED
	15a. DECLASSIFICATION DOWNGRADING SCHEDULE

16. DISTRIBUTION STATEMENT (of this Report)

Approved for public release; distribution unlimited.

17. DISTRIBUTION STATEMENT (of the abstract entered in Block 20, if different from Report)

18. SUPPLEMENTARY NOTES

AFAMRL Contact: Dr. Ints Kaleps, AFAMRL/BBM, Tel. 513/255-3665, AV 785-3665

19. KEY WORDS (Continue on reverse side if necessary and identify by block number)

Axial Stiffness of Shoulder
Biomechanics
Drawer Displacements
Force Applicator with Sonic Emitters
Forced Kinematic Motion
Kinematics with Sonic Emitters
Passive Resistive Forces
Shoulder Complex

20. ABSTRACT (Continue on reverse side if necessary and identify by block number)

This report, first, presents a brief introduction dealing with kinematics measured by means of sonic emitters and a special application of this technique to the shoulder complex. This is followed by a presentation of a new data collection methodology and analysis of the sonic emitters data by utilization of the three most accurate sonic emitters out of six located on the arm cuff of the test subject. Numerical results are provided for three male subjects in the form of plots showing passive resistance of the shoulder complex as functions of drawer displacements of the upper arm for its several orientations with respect to the torso

DD FORM 1 JAN 73 1473 EDITION OF 1 NOV 65 IS OBSOLETE

SECURITY CLASSIFICATION OF THIS PAGE (When Data Entered)

PREFACE

The research work described in this report was performed for the Modeling and Analysis Branch of the Air Force Aerospace Medical Research Laboratory (AFAMRL) at the Wright-Patterson Air Force Base under Technical Consultant Agreement No. 6322-62-17. The research was monitored by Dr. Ints Kaleps, the Chief of the Modeling and Analysis Branch of the AFAMRL and it was administered by Systems Research Laboratories, Inc. in Dayton, Ohio under Contract No. F33615-81-C-0500.

The author acknowledges the able assistance provided by one of his graduate students, Mr. Richard D. Peindl, in various aspects of the research work.

TABLE OF CONTENTS

LIST OF FIGURES

LIST OF FIGURES (CONTINUED)

LIST OF FIGURES (CONTINUED)

LIST OF TABLES

INTRODUCTION

Proper biomechanical descriptions of major human joints are essential for improving the biodynamic response of the multisegmented models of the human body. In a series of technical reports [1-3] and articles [4-18] this author and his associates presented passive and active force and moment response characteristics of major human joints, associated torques about the long-bone axes of these joints and some aspects of joint modeling. It was also established that in multisegmented mathematical models of the human body the most difficult and the least successful modeling of the major articulating joint has been the shoulder complex because of the lack of appropriate biomechanical data as well as the anatomical complexity of the region.

At the initiation of this present research task, a partial set of data existed on the forced kinematic motion (drawer tests) of the shoulder complex of one male subject. Since that time additional data were collected on two more male subjects to provide quantitative results on the variability of the "stiffness" of the shoulder complex dependent upon selected orientations of the upper arm. This report, first, presents a section dealing with kinematics by means of sonic emitters and a special application of this technique to the shoulder complex. This is followed by a presentation of a method developed to analyze the raw sonic emitters data by utilization of the three most accurate sonic emitters out of six located on the arm cuff of the test subject. The final numerical results are provided in the form of plots showing the passive resistance of the shoulder complex versus drawer displacements of the upper arm when the humerus, the long-bone of the upper arm, is forced axially.

KINEMATICS BY MEANS OF SONIC EMITTERS: APPLICATION TO THE SHOULDER COMPLEX

The quantitative determination of the nature of the relative motion between two body segments, which are connected by a complex anatomical joint, is of prime importance to the biomechanician as well as to those in medicine. The simple hinge joint with one degree of freedom and the ball and socket joint with three degrees of freedom are the most popular joints employed in multisegmented mathematical models of the human body. Under physiological and external loads, each articulating human joint can display up to six degrees of freedom to some extent. A good example of a general joint is the shoulder complex which exhibits four independent articulations among the humerus, scapula, clavicle, and thorax. Of course at the shoulder complex, the six degrees of freedom refers to the motion of the humerus relative to a fixed portion of the torso. Since flexing of the rib cage contributes to the overall range of motion of the humerus, our "fixed body" consists of the lower half of the torso (below the T-9 vertebra) and the upper collateral side of the torso (opposite to the shoulder being investigated). The kinematics analysis, which is considered here, is a rigid body analysis. It is very essential to point out, before we proceed further, that no human body segment is a rigid body in the sense defined in mechanics. However, by the judicious use of semi-rigid orthotic shells and various restraints, approximate rigid body conditions were invoked during in-vivo experiments without limiting the natural range of motion of the joint complex.

In this study, we wish to monitor the displacement of a point in the humeral head as well as the orientation of the longitudinal axis of the

humerus. This will, in essence, give us some idea of the displacement of the glenohumeral joint with respect to the torso. If one considers the types of motion possible by the shoulder complex (i.e. sweeping-type motions as well as drawer type motions) it becomes obvious that the permissible locations of the glenohumeral joint define a volume in space relative to the fixed portion of the torso. In addition, the voluntary boundaries of this volume are extended in a variable manner by external loading of the humerus. The role of the sonic digitizer in this kinematics analysis is to: 1) locate the fixed-body origin and define its axis system with respect to the microphone/sensor assembly coordinate system, and 2) to monitor the motion of the humerus with respect to that same axis system. We can then transform the humeral kinematics into the fixed-body system of the torso by means of matrix transformations.

If we select a point (origin) in the moving body segment and establish a local axis system at that origin, then the kinematics of the moving body segment with respect to the fixed reference is fully defined if we can continuously monitor the location of the selected point and the orientation of the local axis system relative to the fixed reference system. This can be accomplished by tracking three points (sonic emitters) fixed on the surface of the moving body segment. One of these three points is selected as the origin and unit vectors in directions from the origin to the other two points, along with their cross product, describe the local axis system.

During the motion analysis it is desirable to know the positions of the three emitters simultaneously at any given instant. Since the emitters are fired sequentially, however, this was not possible. One way to

simulate simultaneous data collection would be to use a "stop-frame" type of motion in which the moving body segment would be motionless during any particular "sweep" of the three emitters. This approach was ruled out for two major reasons: 1) the digitizer cannot take commands from the computer, any pause in the sequential firing order makes it necessary that the digitizer is reset manually, and 2) the necessity of applying steadily increasing loads to the moving body segment makes this technique undesirable. A more tenable solution was to increase the firing rate of the digitizer so that the displacement of the moving body segment during any given sweep of the three emitters would be small compared to the distances between the emitters themselves.

Two major modifications of the data collection system enabled us to maximize the digitizer firing rate. First an IEEE-488 interface in place of the RS-232 interface was installed between the GP6-3D (sonic digitizer) and the PDP-11/34. While the RS-232 allows single line-serial data transmission, the IEEE-488 uses eight lines for bit-parallel byte-serial data transmission. Secondly, the programming of the digitizer's microprocessor was altered so that slant range data were output directly to the computer (with a minimum of formatting) thereby eliminating any preprocessing of the data by the digitizer. Although these changes were very time consuming, we were able to increase the emitter pulse rate from 15 pulses/sec to approximately 60 pulses/sec (i.e. $\approx$ 20 sweeps of 3 emitters each second).

Initial experiments making use of the sonic digitizing technique demonstrated that additional modifications were necessary in our overall

approach. While the data obtained for simple planar motions, with all of the emitters facing the sensor assembly, are quite accurate; more general 3-dimensional-type motions produced data of more questionable accuracy. If the tip of an emitter is rotated away from the sensor assembly, the sound waves must travel around the emitter's base. Likewise, certain rigid body motions either partially or completely block the emitter from the "view" of one or more sensors. These conditions can either alter the slant range data or produce a zero reading depending on the amount of blockage. Therefore it was necessary to: 1) devise some method to check the accuracy of the data obtained, and 2) collect redundant data in order that zero readings from individual emitters would not affect the kinematics analysis. The following section addresses these considerations and describes a new data collection methodology which was developed.

A NEW DATA COLLECTION METHODOLOGY & DATA ANALYSIS

Since the kinematics analysis used in this research is essentially based on vector operations involving several axis systems, the following subscripts are utilized to specify the cartesian coordinate systems and components of the vectors in these coordinate systems:

f: fixed body system

s: sensor assembly axis system

ℓ or (#,#,#): arbitrary or specific arm cuff local axis system, respectively.

Likewise, these same notations are used as superscripts for transformation matrices. For example in the equation,

$$\hat{h}_s = \underline{A}^{sf}\, \hat{h}_f$$

$\underline{A}^{sf}$ is the matrix transformation which specifies the sensor assembly axis system with respect to the fixed body system. The unit vector $\hat{h}$ as shown in Fig. 2 defines direction of the long-bone axis of the humerus.

During the tests, the subject is secured in a chair restraint system which restrains the lower torso, pelvis, and head and also allows the experimenter to position the subject in any desired orientation relative to the sensor assembly. This system is schematically illustrated in Fig. 1. The chair has motor-driven pitch and yaw capabilities and is adjustable to the anthropometry of the subject. In order to conveniently and accurately locate the fixed body system relative to the sensor assembly axis system, a relative axis locator device (RALD) was developed. The RALD, uses four sonic emitters, arranged in a pyramidic fashion, to describe an axis system and origin location in space relative to the sensor assembly. With the fixed body positioned, as desired, with respect to the sensor assembly, the RALD axes are aligned with the fixed body system and position data are obtained for five successive sweeps of the RALD's four emitters. The three emitters which produce the most consistent readings are used to calculate $\overline{R}_s$ and $\underline{B}^{fs}$, where,

$\overline{R}_s$ = a vector describing the RALD origin

$\underline{B}^{fs}$ = a transformation matrix defining the fixed body system with respect to the sensor assembly system

Therefore:

$$\overline{R}_f = \underline{B}^{fs}\, \overline{R}_s$$

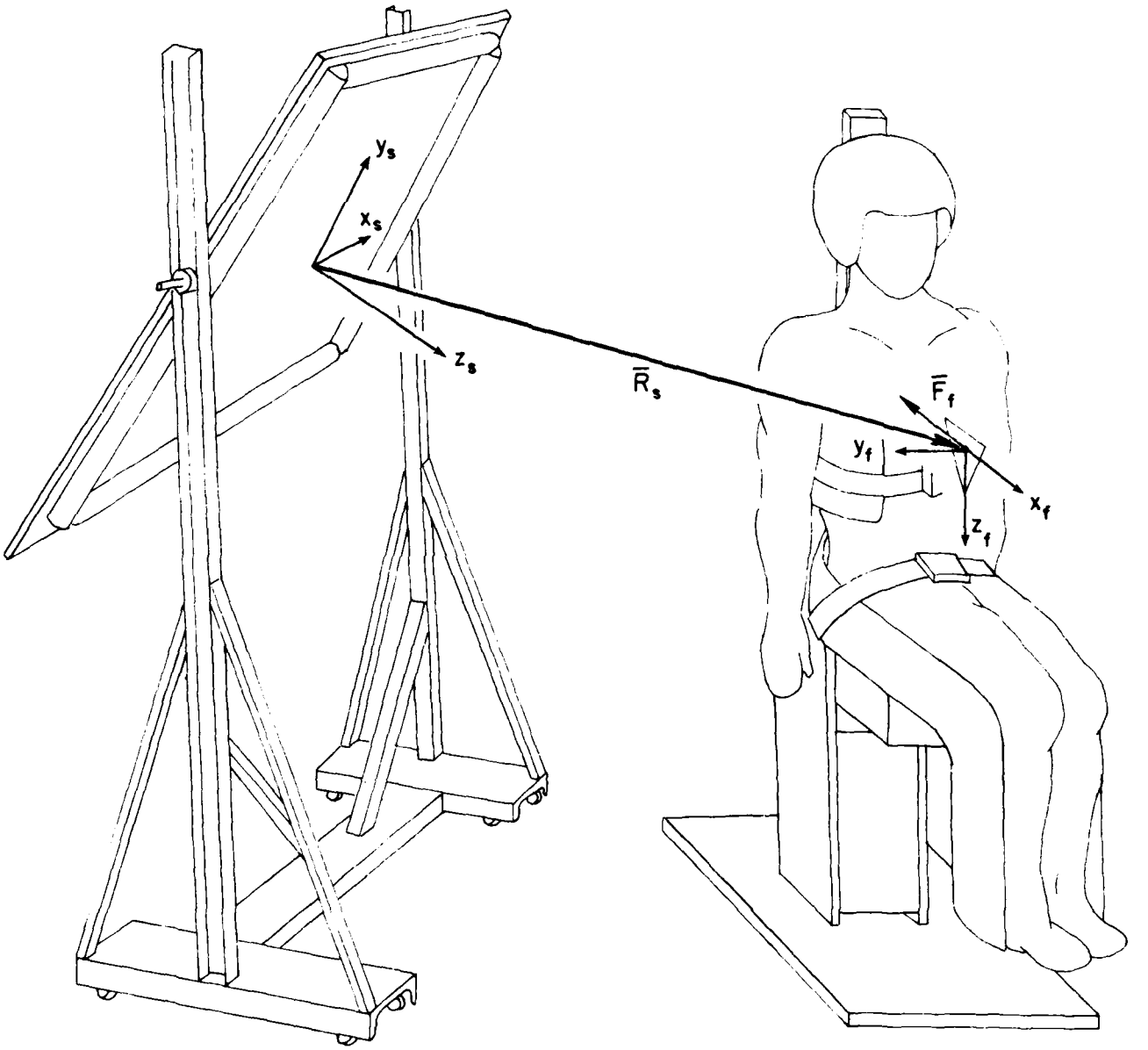

Fig. 1. Schematic drawing of experimental setup and coordinate systems.

Inversely, the sensor assembly axis system can always be determined with respect to the fixed body system by:

$$\begin{pmatrix} x \\ y \\ z \end{pmatrix}_s = \underline{B}^{sf} \begin{pmatrix} x \\ y \\ z \end{pmatrix}_f = \left(\underline{B}^{fs} \right)^T \begin{pmatrix} x \\ y \\ z \end{pmatrix}_f$$

There is, therefore, no need to measure any sensor board or chair orientation angles as was done previously. This approach is very flexible from a data acquisition point of view. Physical dimensions of the subject are used to specify a vector from the RALD origin to the actual fixed body origin. This vector $\overline{F}_f$, along with $\overline{R}_f$ and $\underline{B}^{sf}$ are stored in a computer data file for use during the kinematic analysis program. This procedure is easily repeated any time that the fixed body is moved with respect to the sensor assembly. Next we address the application of sonic emitters to the moving body segment, i.e. the upper arm.

In order to mount emitters on the upper arm, an orthotic cuff (schematically shown in Fig. 2) was used. This cuff consists of a semi-rigid, cylindrical, plastic shell, which is encased in a thin rubber envelope. It extends about three-quarters of the way around the upper arm. Velcro straps, at the top and bottom of the cuff, allow it to be tightly secured circumferencially. The cuff's length was selected based on the subjects' upper arm dimensions so that the top strap rides in the bicipital groove (immediately below the major body of the deltoid muscle), and the bottom strap rides in the antecubital fold (at the distal end of the biceps, above the elbow). This configuration, along with the static friction of the rubber/skin interface, makes the cuff suprisingly secure both

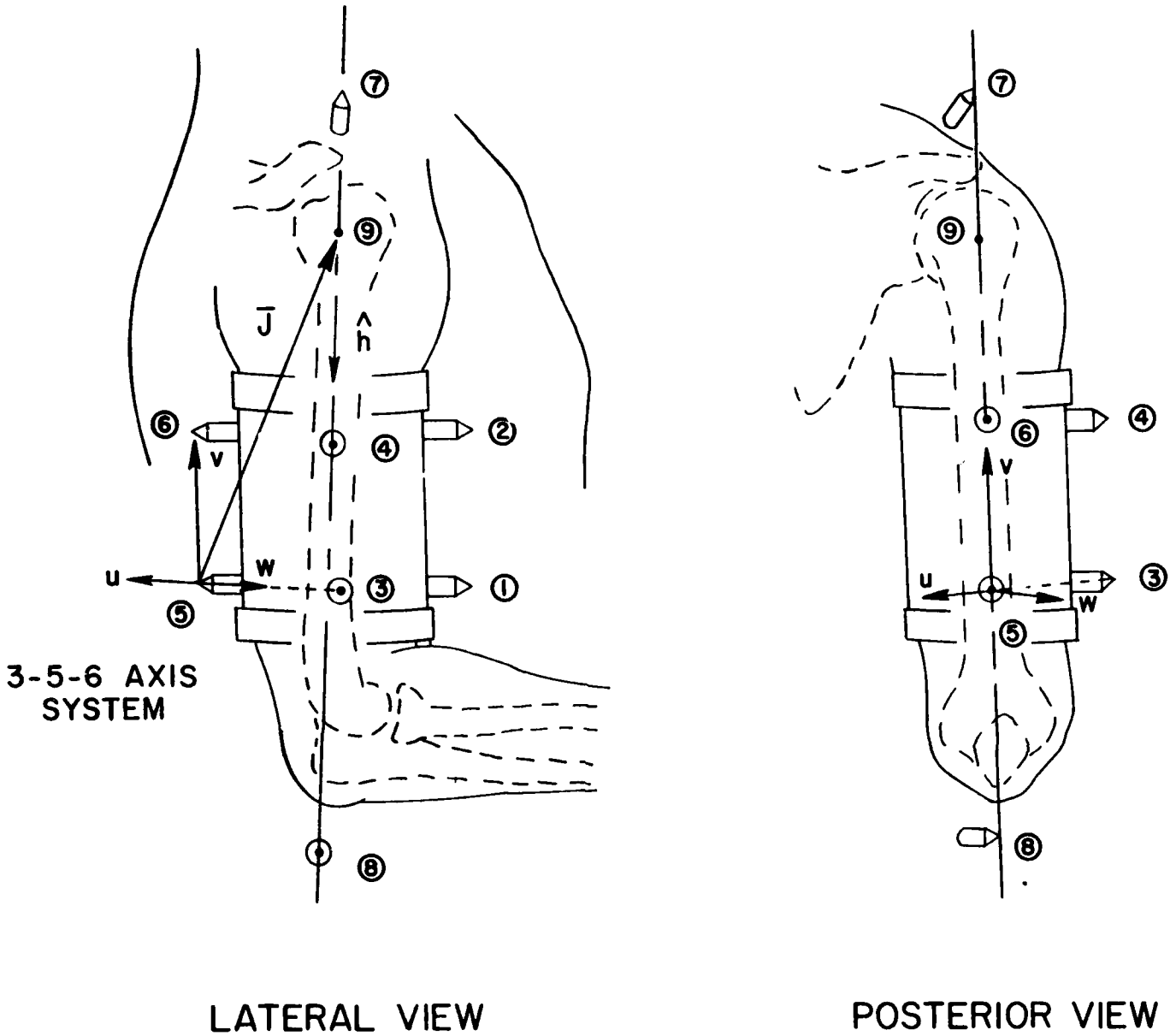

Fig. 2. The upper arm cuff, its sonic emitters and one of the local axis systems defined by emitters 3,5 and 6.

longitudinally and circumferentially. Six sonic emitters are affixed to the cuff as shown in Fig. 2. Since only three emitters are needed to describe the location and orientation of the upper arm, three emitters can be totally blocked from sensor view without losing kinematic data. A selection of the "most accurate" three emitters is made in cases where four, five, or all six emitters produce non-zero data. This selection process will be explained shortly. For the purposes of the discussion to follow, we will denote one sweep of the six arm cuff emitters by the digitizer as a record.

Before a kinematic test is performed, an initialization procedure is performed to establish baseline data on the locations of the six cuff emitters relative to the humerus. Let us consider the six cuff emitters as points on the upper arm. Referring to Fig. 2, the procedure is as follows. The elbow is flexed to 90°, and one emitter is positioned above the acromion (pt. 7) and another emitter is placed below the olecranon process of the ulna (pt. 8). A data file which contains the relative coordinate locations of these eight emitters is collected. A unit vector, $\hat{h}_s$, in the direction from pt. 7 to pt. 8, defines the long-bone axis of the humerus. Next, knowing the coordinate location of pt. 7, we use $\hat{h}_s$ and a pre-determined length based on the subject's dimensions, to calculate the location of pt. 9. The point 9 is an approximation of the center of a sphere whose surface defines the articulating surface of the humeral head. This, therefore, also approximates the center of a sphere containing the glenoid cavity surface on the scapula. The point 9 is what we define as our glenohumeral joint center, whose displacement is calculated in the kinematic analysis.

Turning our attention to the six arm cuff emitters, we note that there are 20 independent combinations of three emitters (triads) which can be used to describe the kinematics of the upper arm. These twenty local systems are denoted as (a,b,c) axis systems, where a, b, and c refer to the cuff emitter numbers which are used in the grouping. A series-type representation can be used to designate the numbered sequences for the local systems by:

$$\sum_{a=1}^{4}\left(\sum_{b=a+1}^{5}\left(\sum_{c=b+1}^{6}(a,b,c)\right)\right)$$

In the above equation the summation-type symbols are used only to indicate how the notational sequence is incremented, and are not meant to infer any summation operation of terms as in a series. This notational scheme insures that all six arm cuff emitters are included in the triad groupings and that no triad is a permutation of any other triad. For the convenience of ordering with respect to computer calculations the triad sequences are labelled 1 through 20 according to:

Triad #	Triad Sequence
1	(1,2,3)
2	(1,2,4)
•	•
•	•
•	•
20	(4,5,6)

For any of these local axis systems, emitter b is the origin, a unit vector in the direction from a to b describes the u-axis, a unit vector directed

from b to c denotes the v-axis, and the cross product of $\hat{u} \times \hat{v}$ is $\hat{w}$ which describes the w-axis. Figure 2 shows the (3,5,6) axis system as an example. Although (3,5,6) coordinate system is an orthogonal system; in general, the local axis systems defined by the triad sequence do not necessarily result in an orthogonal system. For example, (1,3,6) is not an orthogonal coordinate system since $\hat{v}$ is not perpendicular to $\hat{u}$. However, it is an easy task to define a new $\hat{v}$ such that $\hat{v} \perp$ to $\hat{u}$ by shifting the origin of the coordinate system along the unit vector $\hat{u}$. Thus, all local axis systems become an orthogonal one. Note that the x, y, and z components of $\hat{u}$, $\hat{v}$, and $\hat{w}$ compose a direction cosine matrix given by:

$$\underline{L}^{(3,5,6)s} = \begin{bmatrix} u_x & u_y & u_z \\ v_x & v_y & v_z \\ w_x & w_y & w_z \end{bmatrix}$$

This matrix defines the local (3,5,6) system relative to the x,y,z axis system of the sensor assembly. Referring again to Fig. 2 if we now calculate the vector from pt. 5 to pt. 9, $(\overline{J}_s)$, we can then locate the joint center with respect to the local system by:

$$\overline{J}_{(3,5,6)} = \underline{L}^{(3,5,6)s}\, \overline{J}_s$$

and likewise:

$$\hat{h}_{(3,5,6)} = \underline{L}^{(3,5,6)s}\, \hat{h}_s$$

In the initialization computer program, vectors locating the joint center and describing the humeral long axis are calculated for all twenty

axis systems and this information is placed in a data file. The initialization program, however, also establishes our "accuracy criteria" for local triad selection. One must realize that during a kinematic test we do not know ahead of time which three emitters will provide the most accurate description of the rigid body location/orientation for any given record. During the initialization procedure, however, we establish a "best condition" data set that records the relative positions of the six cuff emitters. We then, in turn, use these data to calculate the relative orientations and locations of the twenty local axis systems with the arm cuff/arm in optimal view of the sensor assembly.

For any two axis systems (i.e. the i-th and j-th axis systems, where i and j are between 1 and 20) we calculate the transformation matrices with respect to the sensor assembly axis system:

$$\begin{pmatrix} x \\ y \\ z \end{pmatrix}_i = \underline{T}^{is} \begin{pmatrix} x \\ y \\ z \end{pmatrix}_s \quad \text{and} \quad \begin{pmatrix} x \\ y \\ z \end{pmatrix}_j = \underline{T}^{js} \begin{pmatrix} x \\ y \\ z \end{pmatrix}_s$$

Therefore, the relationship of the j-th system with respect to the i-th system is given by

$$\begin{pmatrix} x \\ y \\ z \end{pmatrix}_i = \underline{T}^{is} \left(\underline{T}^{js} \right)^{-1} \begin{pmatrix} x \\ y \\ z \end{pmatrix}_j = \underline{T}^{ij} \begin{pmatrix} x \\ y \\ z \end{pmatrix}_j$$

where $\underline{T}^{ij}$ is 3x3 transformation matrix describing the i-th system with respect to the j-th system. The transformation matrices relating each of the 20 local systems to every other system are calculated in this manner, thereby arriving at 190 direction cosine matrices. Only transformations in one direction are calculated since it is obvious that:

$$\underline{T}^{ij} = \left(\underline{T}^{ji} \right)^{-1}$$

These matrix relationships are stored in the same data file, along with the joint center vectors and the humeral axis vectors for the twenty local systems. The final step in the initialization procedure/program is to calculate the distances between the various local axis systems and to store these data along with the previously mentioned information. Note that these initial or baseline data are obtained with the arm cuff emitters and humeral axis emitters in optimal view of the sensor assembly.

For a typical test, with the upper arm in motion, the choice of the "most accurate" local system is made during the kinematic analysis on a record-by-record basis. For each record of kinematic data, the coordinate data of the six cuff emitters are once again used to calculate the direction cosine matrices describing the local axis systems with respect to the sensor assembly system. These new (kinematic) local axis systems are, in turn, used to obtain the matrix transformations (interrelationships) between the local axis systems. Let us designate these matrix transformations with $\underline{T}^{ij}_{\text{kinematic}}$.

The transformation matrices obtained from the kinematic data will differ from their initialized counterparts for the following reasons:

1) Since the emitters do not fire simultaneously, the "apparent" axis system for a given emitter triad utilizes data obtained at three different times.

2) As emitters are rotated away from the "view" of the sensor assembly, the acoustic pulse may still be detected, but the

distance measurements are dilated because the acoustic wave needs to travel around part of the emitter itself.

3) Acoustic blockage similar to item 2 may be caused by the location of part of an object such as a body segment between the emitters and the sensor assembly. Obviously, the object affects the acoustic field which is produced by the emitter pulse and will cause dilations in the distance measurements.

4) The reproducibility of the measurements varies ± 1 in the last significant digit which corresponds to ± .1 mm or ± .1% of the distance measured.

Therefore, during data analysis, it is the deviation from the predetermined, initialized axis system interrelationships that constitutes the selection procedure for establishing the local axis system which best describes the moving body segment location and orientation. If there were no errors in measurements, and a "stop-motion" type of sweeps of the cuff emitters were possible, then we should obtain the equality:

$$\underline{T}^{ij}_{\text{kinematic}} = \underline{T}^{ij}_{\text{initial}}$$

or

$$\left(\underline{T}^{ij}_{\text{kinematic}}\right)\left(\underline{T}^{ij}_{\text{initial}}\right)^{-1} = [I]$$

where [I] is the 3x3 identity matrix. This, however, is not the case, and a general matrix [G] with off-diagonal terms is obtained. Therefore:

$$\left(\underline{T}^{ij}_{\text{kinematic}}\right)\left(\underline{T}^{ij}_{\text{initial}}\right)^{-1} = [G] = \begin{bmatrix} g_{11} & g_{12} & g_{13} \\ g_{21} & g_{22} & g_{23} \\ g_{31} & g_{32} & g_{33} \end{bmatrix}$$

The matrix [G], thus, represents an "apparent" rotation of the i-th axis system with respect to the j-th axis system. The angle of rotation between these two coordinate systems is given by [24]:

$$\gamma_{ij} = \cos^{-1}\left(\frac{1}{2}\left[g_{11} + g_{22} + g_{33} - 1\right]\right)$$

This "apparent" or perceived rotation, which results from the measurement error factors previously mentioned is denoted as the skew angle error, γ_{ij}. Note that the skew angle error will affect joint center calculations. If we use an average distance of 20 cm from a local axis system to the joint center and a skew angle error of 0.20 degrees, the magnitude of the maximum error of $(\delta_{ij})_{sk}$ in the joint center computation will be

$$(\delta_{ij})_{sk} = 20 \sin(0.20) = 0.070 \text{ cm}$$

In this way, $(\delta_{ij})_{sk}$ values are calculated for all 190 matrix interrelationships. If we likewise compare the distances between origins for the kinematic data record versus the initialized data we can obtain an error that can be induced in the joint center calculation due to apparent local axis system dislocation, $(\delta_{ij})_d$, where:

$$(\delta_{ij})_d = D_{ij_{\text{kinematic}}} - D_{ij_{\text{initial}}}$$

with $D_{ij_{\text{kinematic}}}$ and $D_{ij_{\text{initial}}}$ as the intra-origin distance between the i-th and j-th system origins for the kinematic and initialized records,

respectively. Having now calculated $(\delta_{ij})_{sk}$ and $(\delta_{ij})_{d}$ for all of the local axis system interrelationships, a least-squares analysis is performed to select the local axis system which minimizes the interrelational errors. For each i-th system a $(\delta_i)_{avg}$ is obtained from:

$$\left(\delta_i\right)_{avg} = \sum_{j=1}^{20} \frac{1}{19} \left\{ \left(\delta_{ij}\right)_{sk}^2 + \left(\delta_{ij}\right)_{d}^2 \right\}^{1/2}, \text{ for } i \neq j$$

From a probability standpoint, the system having the smallest $(\delta_i)_{avg}$ is likely to be the most accurate with respect to the sensor assembly. A physical interpretation is that the system, thus selected, perceives the least amount of change among the systems surrounding it; likewise systems that perceive large changes in many surrounding systems are more likely to be in error themselves. Having thus selected the "best-fit" triad of emitters from the six arm cuff emitters we denote the axis system that they describe with respect to the sensor assembly by means of the transformation matrix $\underline{L}^{\ell s}$. The transformation $\underline{L}^{\ell s}$ is used, along with the retrieved initialized data on the joint center vector and humeral axis vector for that particular axis system, to help calculate the joint center location and humeral axis orientation with respect to the fixed body segment.

Referring to Fig. 3, the vector to the origin of the selected local system on the arm cuff is denoted as $\overline{C}_s$. By inspection, the vector from the fixed body origin to the joint center $(\overline{G}_f)$ can be calculated by:

$$(\overline{G})_f = (-\overline{F} - \overline{R} + \overline{C} + \overline{J})_f$$

where $\overline{F}_f$ is given in the fixed body system, and:

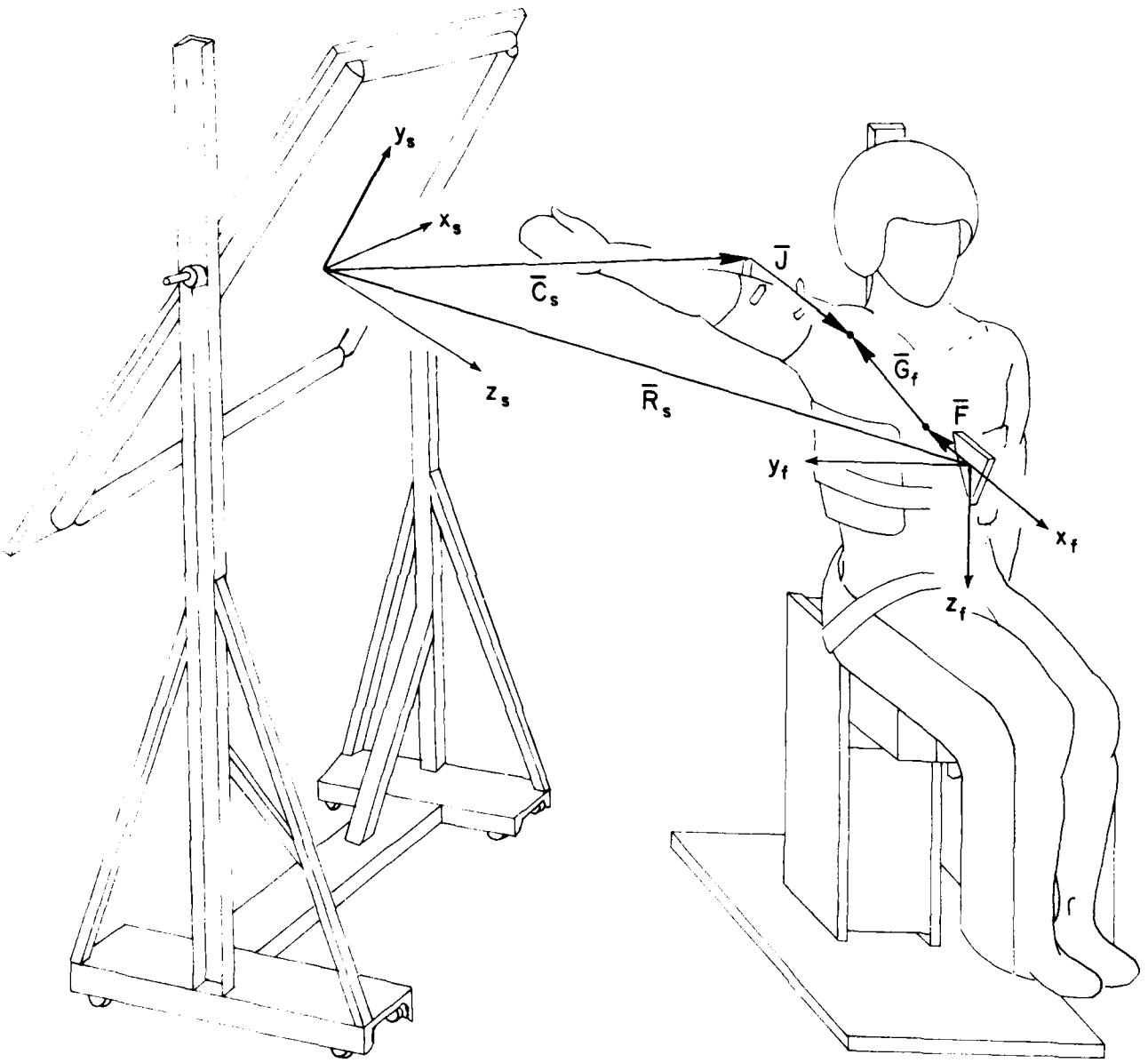

Fig. 3. Definition of various vectors.

$$\overline{R}_f = \underline{B}^{fs}\,\overline{R}_s$$

$$\overline{C}_f = \underline{B}^{fs}\,\overline{C}_s$$

$$\overline{J}_f = \underline{B}^{fs}(L^{\ell s})^T\,\overline{J}_\ell$$

and likewise,

$$\hat{h}_f = \underline{B}^{fs}(L^{\ell s})^T\,\hat{h}_\ell$$

This procedure is repeated for each record; each time a new joint center location and humeral axis orientation are computed with respect to the fixed body segment (the torso). Since these records determine the instantaneous positions and orientations of the moving body segment, the upper arm, the kinematics of the moving body segment is thus fully known.

To complete the data analysis one must describe the function of the force applicator which can be seen in Fig. 4 showing a subject in position for superior-inferior drawer testing. The force applicator has two functions: (1) to determine the direction and the magnitude of the force application, and (2) to determine the location of the force application on the moving body segment with respect to the sensor assembly axis system. This is accomplished by monitoring three strategically located sonic emitters on the force applicator. The force applicator actually has four emitters (no. 1 is located on the opposite side from no. 3), but only three are in view of the sensor assembly for any given test. For the forced motion tests, the subject and sensor assembly are arranged in such a way as to provide optimum tracking of the force applicator. For this reason, redundant

Fig. 4. Subject in position for superior-inferior drawer tests.

emitters, as in the case of the arm cuff, were not necessary. Since the exact relative positions of the three sonic emitters are known, sufficient information exists for a vector analysis to determine both the location and direction of the applied force.

If we refer to Fig. 5, we see that the arrangement of the emitters allows us to readily specify the orthogonal axis system of the transducer. Initially, a unit vector in a direction from pt. 1 to pt. 2 defines the z-axis of the transducer. Next, pt. 4 is calculated as the mid-point between points 2 and 3. Let d_1 specify the magnitude of the vector from pt. 2 to pt. 3, then the vector $\overline{P}_s$ is obtained by:

$$\overline{P}_s = \left(\frac{d_1}{2} (\hat{u}_{12} \times \hat{u}_{23}) \right)_s$$

where the subscript s, as before, denotes that the vectors in the above equation are with respect to the sensor assembly axis system. Using this same convention, we denote the position vector which locates the number 2 emitter as $(\overline{r}_2)_s$. Therefore, by inspection of Fig. 5, we see that the location of pt. 5 (on the longitudinal axis of the force applicator) is given by:

$$(\overline{r}_5)_s = (\overline{r}_2)_s + \frac{d_1}{2} (\hat{u}_{23})_s + \overline{P}_s$$

and the location of pt. 6 (the point of force application) is given by:

$$(\overline{r}_6)_s = (\overline{r}_5)_s + d_2(\hat{u}_{12})_s$$

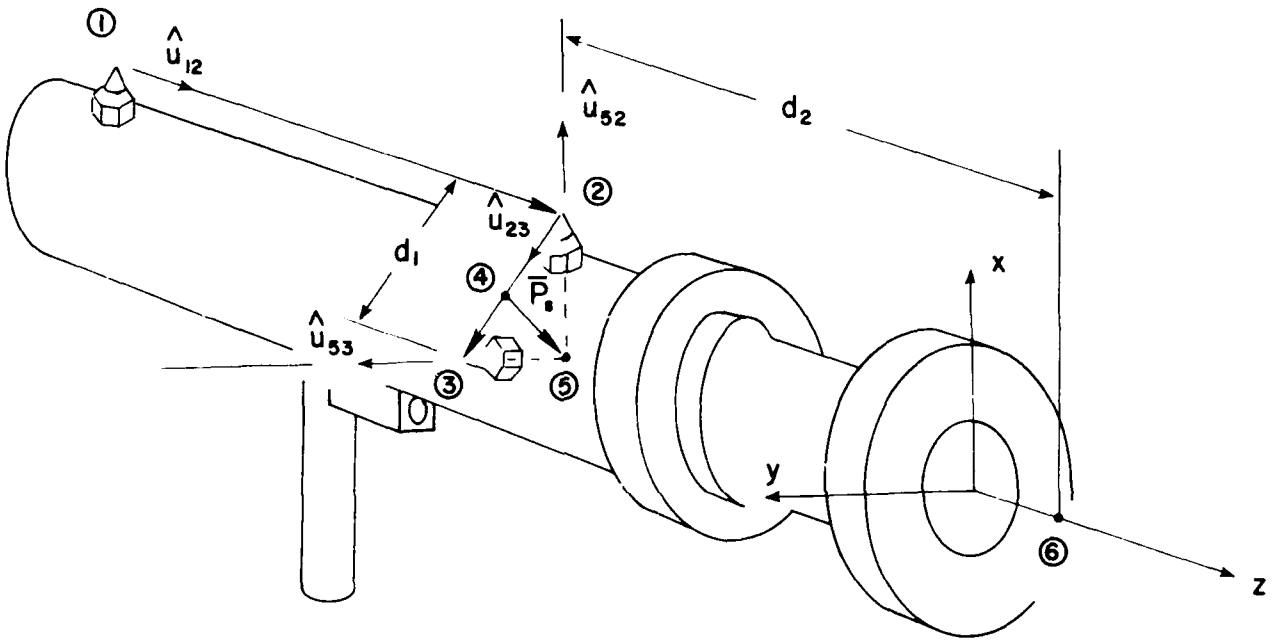

Fig. 5. Arrangement of the sonic emitters and definitions of various vectors on the force applicator.

Note that unit vectors from pt. 5 to points 2 and 3 define the transducer's x and y axes, respectively, with respect to the sensor assembly axis system. Since both the point of force application and the transducer axes are now known with respect to the sensor assembly system, these data are easily transformed into the fixed body system as was done with the arm cuff data. Once again, the data are updated on a record by record basis.

RESULTS

Using the concepts presented in the previous section the data obtained from a number of tests which were performed for determination of the passive resistance of the shoulder complex to forced (drawer-type) motions were analyzed. In these tests the upper arm was forced axially for a variety of upper arm orientations with respect to torso. Before we present the results of the data analysis we will briefly describe the testing procedure.

During the tests, the subject is secured in the chair restraint system which allows unimpeded movement of the shoulder complex. After the initialization procedure is completed, and the fixed body is located with respect to the sensor assembly by means of the RALD, the force applicator is fixed to the arm by means of a rigid cuff extension so that the force can be applied comfortably along the humeral axis. In addition, the rigid cuff places the upper arm in a position of approximately 25° of medial rotation. This position is near the mid-range of the shoulder medial-lateral rotation limits and is a comfortable position for the subject.

For each upper arm orientation defined in the next paragraph, the arm is forced proximally and then distally along its longitudinal axis. Before each test, the subject was asked to allow his shoulder complex to assume its most comfortable, "natural" position. This established the neutral position for each drawer. During the tests the subjects were instructed to avoid muscular resistance, and each test was terminated when the subject expressed discomfort. Three male subjects were tested* at six positions of the upper arm orientations. Subjects were university students with no special training in athletics. Selected anthropometric measurements of the subjects are given in Table I. The definitions of the anthropometric measurements provided in Table I can be found in [3 & 13]. The six positions can be defined by means of θ and ϕ angles. The θ angle refers to the angle between the z-axis of the torso and the long-bone axis of the upper arm; this angle also defines the shoulder flexion-extension in the sagittal plane. The ϕ angle refers to the angle between the projection of the long-bone axis of the upper arm on the xy-plane and the x-axis; the positive and negative values of this angle also define the shoulder abduction and adduction, respectively.

The test data were analyzed and presented for the following six positions of the upper arm: 1) $\theta = 0°$, $\phi = 0°$ which corresponds to the inferior-superior drawer test as shown in Fig. 4; 2) $\theta = 90°$, $\phi = 0°$ which corresponds to anterior-posterior drawer test in the sagittal plane; 3) $\theta = 90°$, $\phi = 30°$; 4) $\theta = 90°$, $\phi = 60°$; 5) $\theta = 90°$, $\phi = 90°$ which

---

* The testing was conducted in conformance with the Human Subject Program Guidelines established by the Ohio State University Human Subject Review Committee.

TABLE I

SELECTED ANTHROPOMETRY OF SUBJECTS 1, 2, 3
(ALL LENGTH DIMENSIONS ARE IN CM)

	1	2	3
WEIGHT (NEWTONS)	787.6	851.9	816.1
STATURE	188.6	185.5	186
SHOULDER CIRCUMFERENCE	115	126.4	116.8
WAIST CIRCUMFERENCE	96	101.6	99
WRIST CIRCUMFERENCE	17	17.8	17.6
LOWER ARM CIRCUMFERENCE	29.8	29.8	28.9
BICEPS CIRCUMFERENCE	32.2	37.1	32
THIGH, UPPER CIRCUMFERENCE	57.5	57.1	57.5
THIGH, LOWER CIRCUMFERENCE	43	40.6	44.5
CALF CIRCUMFERENCE	41	40.6	38
ANKLE CIRCUMFERENCE	26	27	26.5
FOREARM-WRIST LENGTH	23.5	21.5	21.5
SHOULDER-ELBOW LENGTH	41	38.5	38.5
SHOULDER HEIGHT, SITTING	67.5	67	68.5
SITTING HEIGHT	97.2	97	94
SHOULDER BREADTH	50	50.5	47
CHEST BREADTH	34.5	35	33
CHEST DEPTH	23	23	22
WAIST DEPTH	20.5	22.5	21
BUTTOCK-KNEE LENGTH	66	62	64
BUTTOCK-POPLITEAL LENGTH	54.5	50.8	53.5
KNEE HEIGHT, SITTING	61	58.5	61.5
ELBOW-TO-ELBOW BREADTH	46.5	48	47.5
HIP BREADTH SITTING	41	37	38
KNEE-TO-KNEE BREADTH, SITTING	25	25.5	22.5

corresponds to medio-lateral drawer test in the frontal plane; and 6) $\theta = 90°$, $\phi = 115°$. The numerical results for these are presented in the form of plots in Figs. 6-23 showing the passive resistance of the shoulder complex as a function of drawer displacement of the upper arm along its long-bone axis. In these plots the ordinate represents, in Newtons, the magnitude of the axially applied force and the abscissa represents, in centimeters, the computed components of the joint center displacement along the force application direction. The force and displacement values were computed on a record by record basis. In addition, for each record, the average skew error and average intra-origin error for the local axis system that was selected to describe the upper arm position were computed, and displayed on the computer printout. These average errors pertain to the "apparent" errors in all the i-th local systems with respect to the j-th system which is selected for use in joint center calculations. For the presented results, the average skew error was less than .45 degrees and the average intra-origin error was less than .15 centimeters.

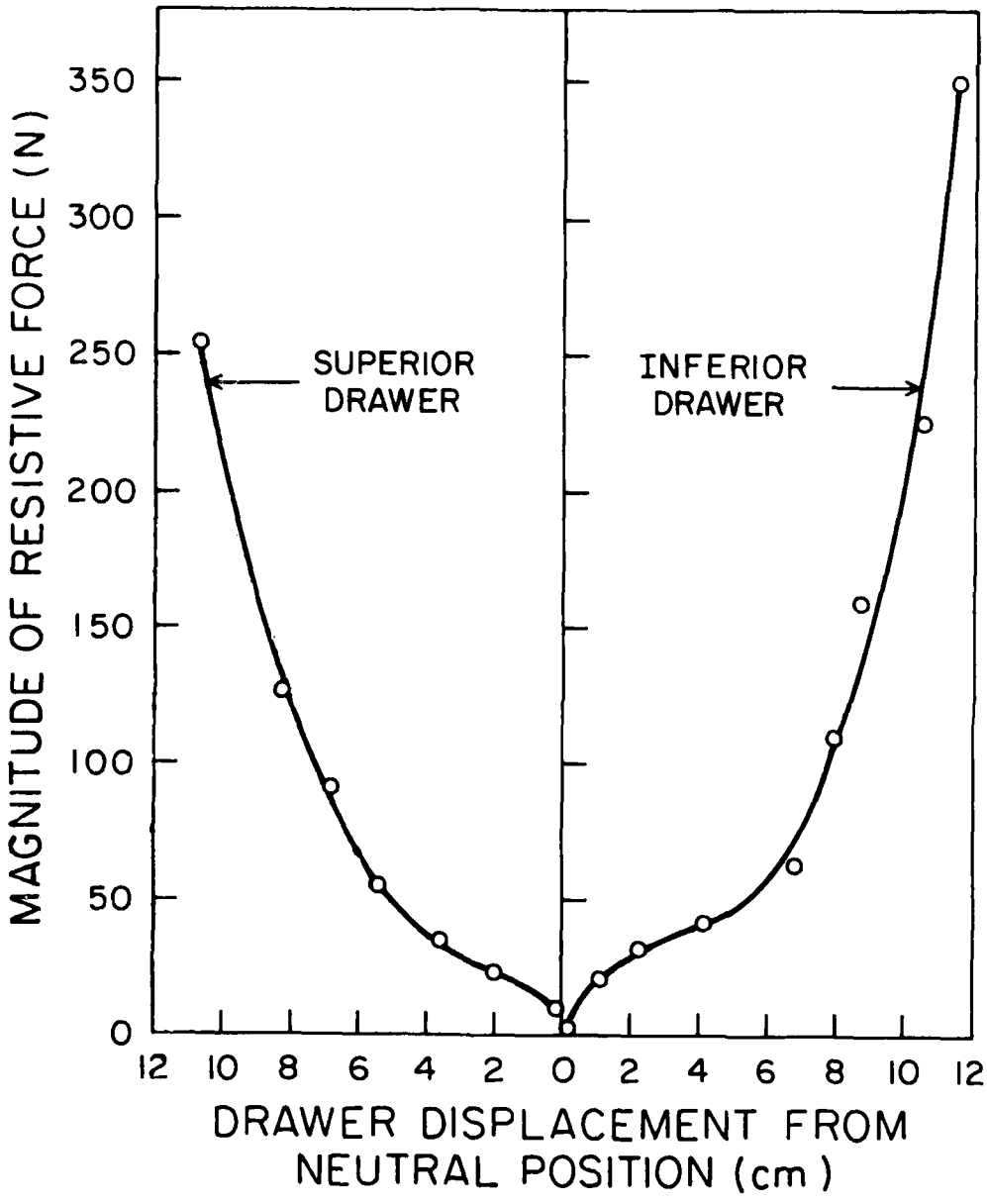

Fig. 6. Passive resistive force versus drawer displacement for the superior-inferior drawer test of the shoulder complex of the first subject for the upper arm orientation along torso ($\theta = 0°$, $\phi = 0°$).

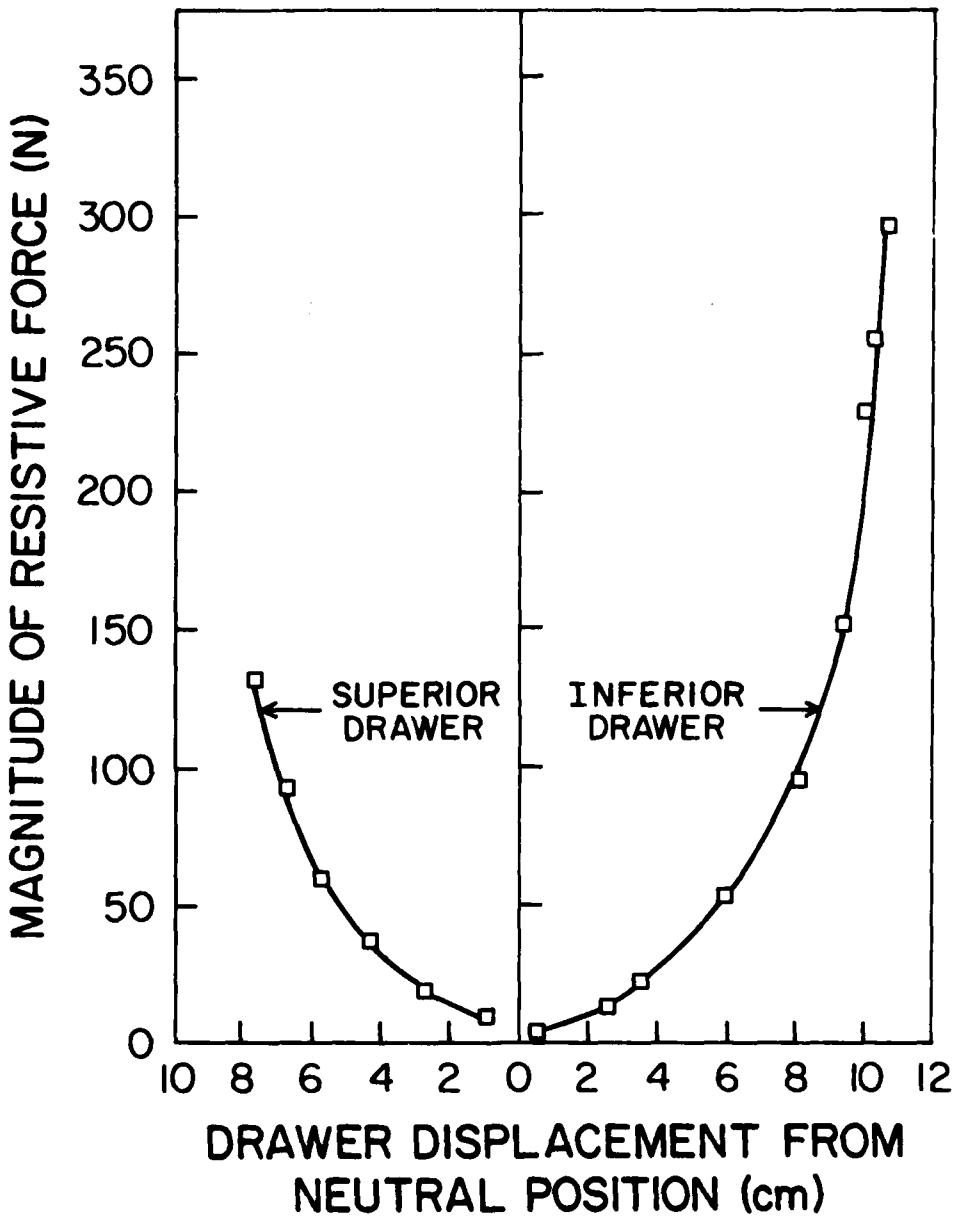

Fig. 7. Passive resistive force versus drawer displacement for the superior-inferior drawer test of the shoulder complex of the second subject for the upper arm orientation along torso ($\theta = 0°$, $\phi = 0°$).

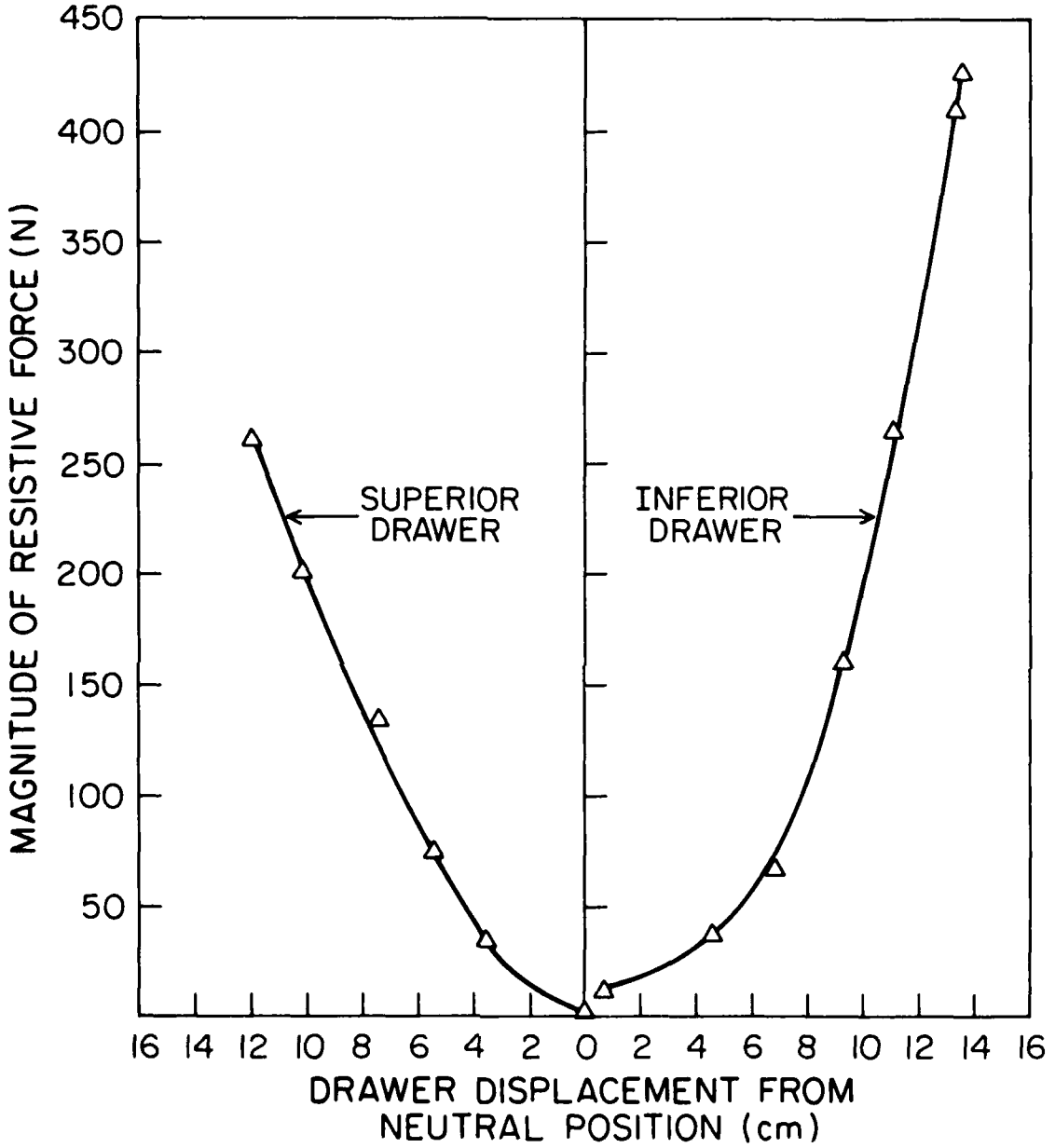

Fig. 8. Passive resistive force versus drawer displacement for the superior-inferior drawer test of the shoulder complex of the third subject for the upper arm orientation along torso ($\theta = 0°$, $\phi = 0°$).

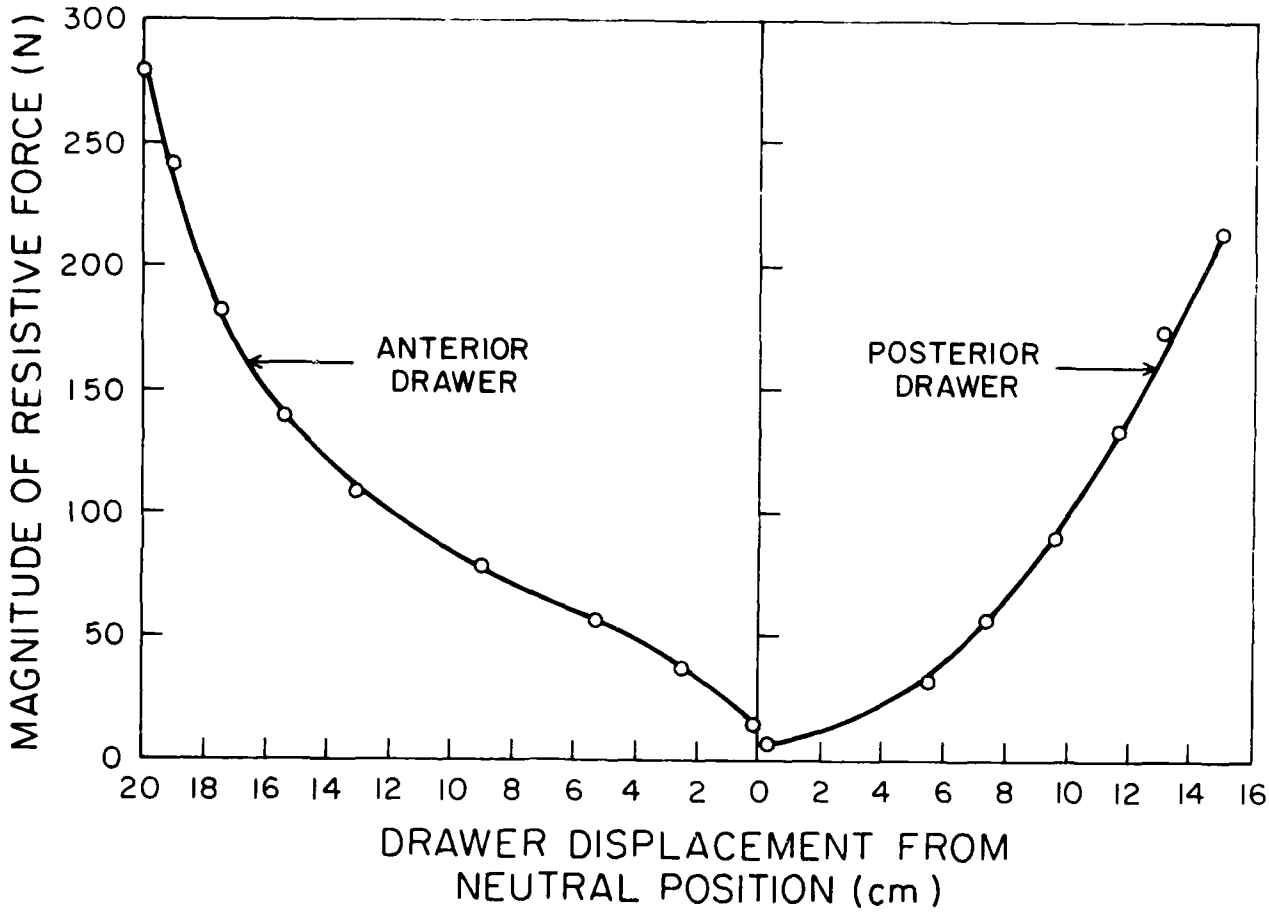

Fig. 9. Passive resistive force versus drawer displacement for the anterior-posterior drawer test of the shoulder complex of the first subject ($\theta = 90°$, $\phi = 0°$).

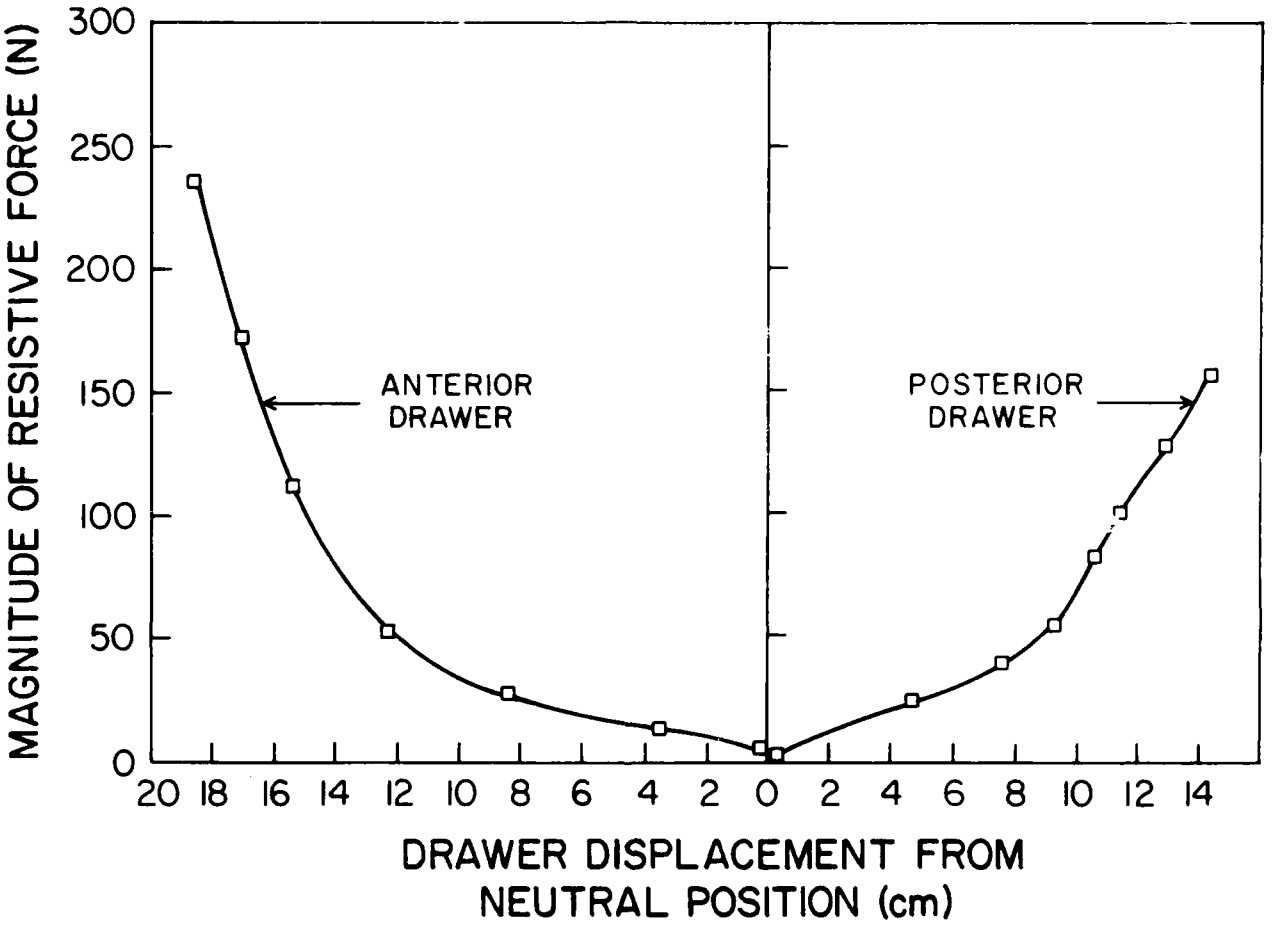

Fig. 10. Passive resistive force versus drawer displacement for the anterior-posterior drawer test of the shoulder complex of the second subject ($\theta = 90°$, $\phi = 0°$).

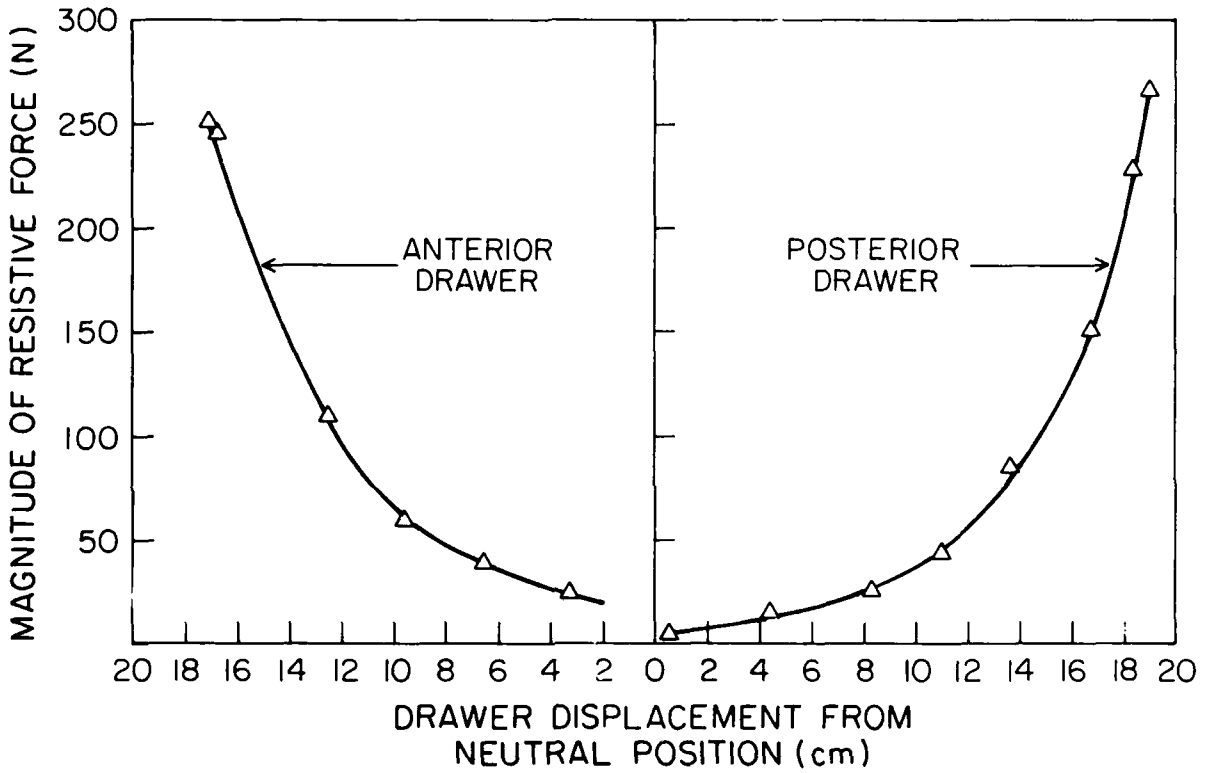

Fig. 11. Passive resistive force versus drawer displacement for the anterior-posterior drawer test of the shoulder complex of the third subject ($\theta = 90°$, $\phi = 0°$).

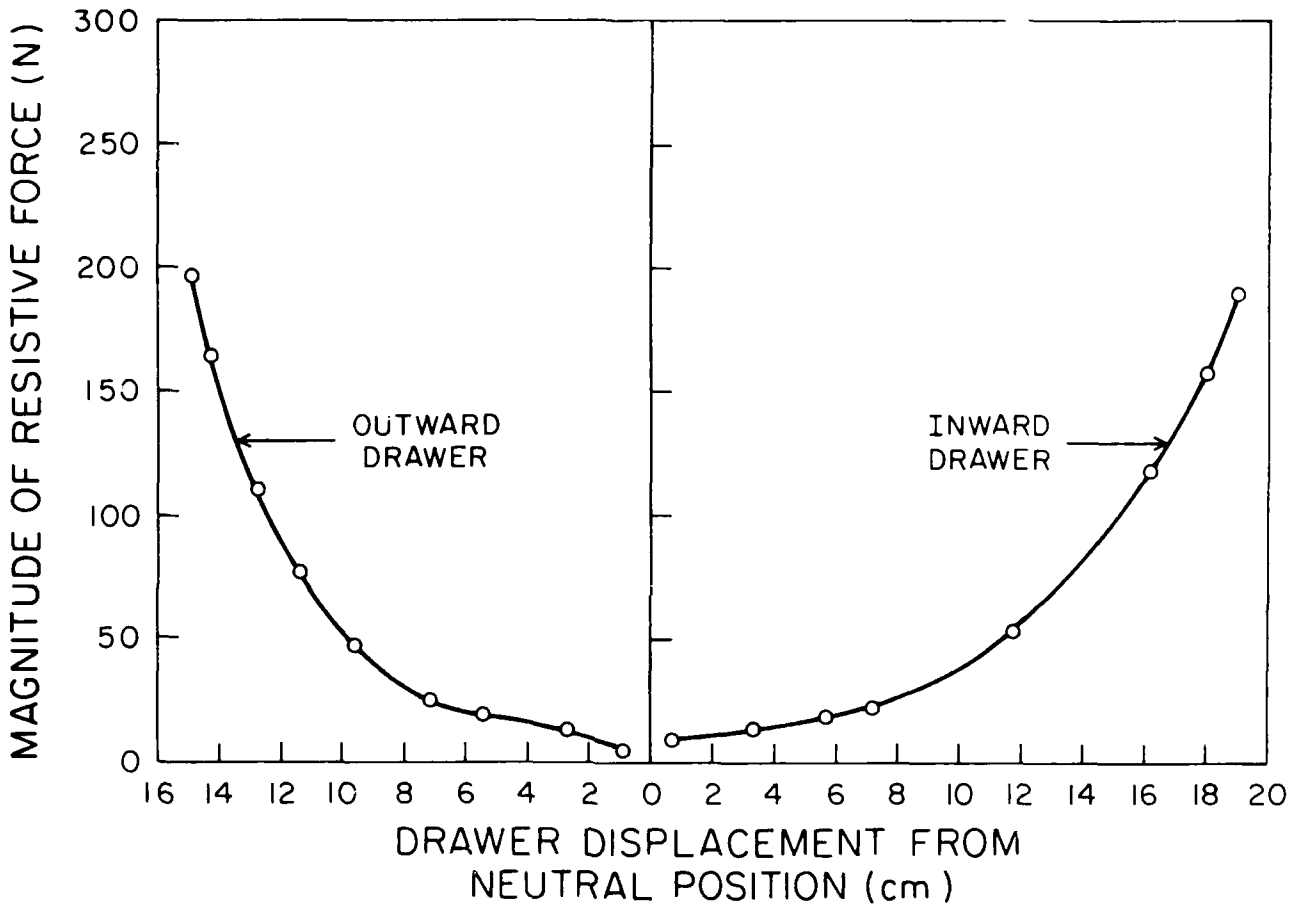

Fig. 12. Passive resistive force versus drawer displacement of the shoulder complex of the first subject for the $\theta = 90°$, $\phi = 30°$ upper arm orientation.

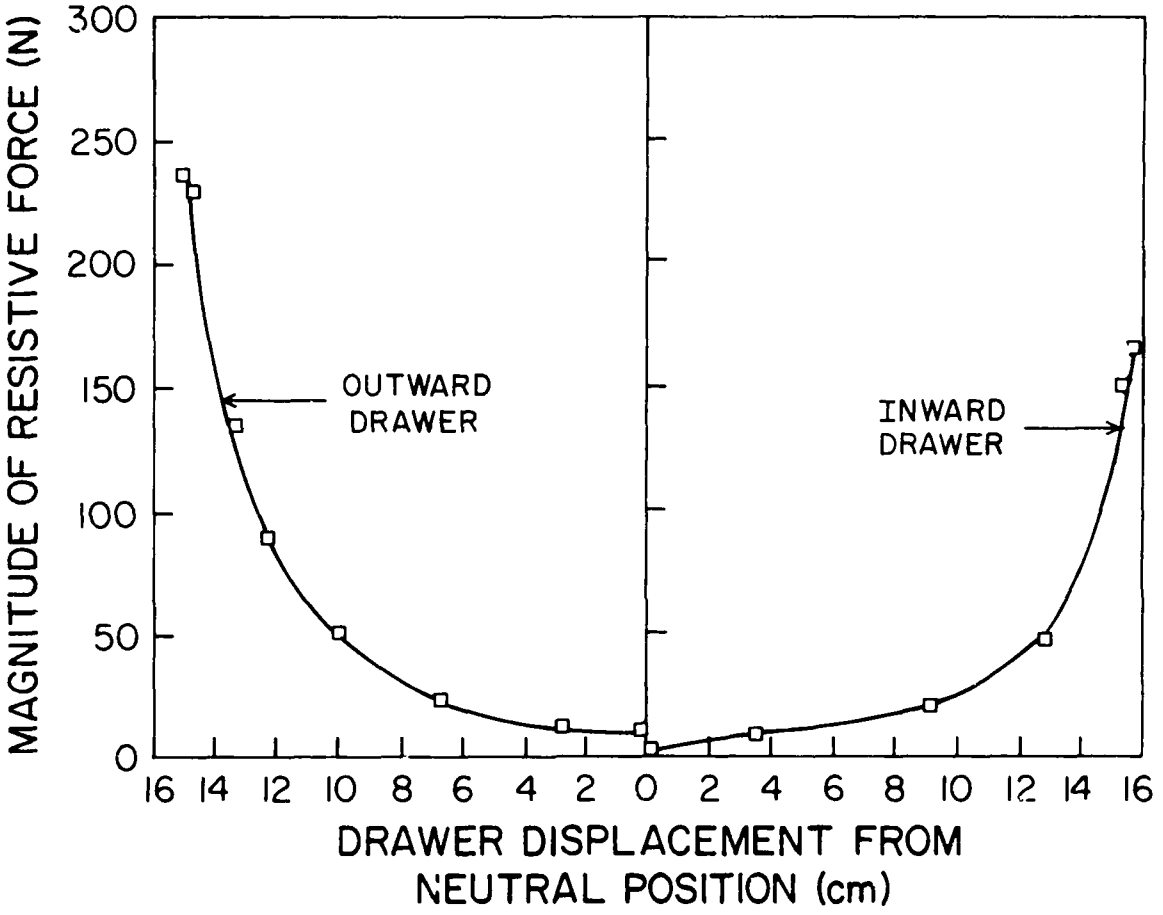

Fig. 13. Passive resistive force versus drawer displacement of the shoulder complex of the second subject for the $\theta = 90^{\circ}$, $\phi = 30^{\circ}$ upper arm orientation.

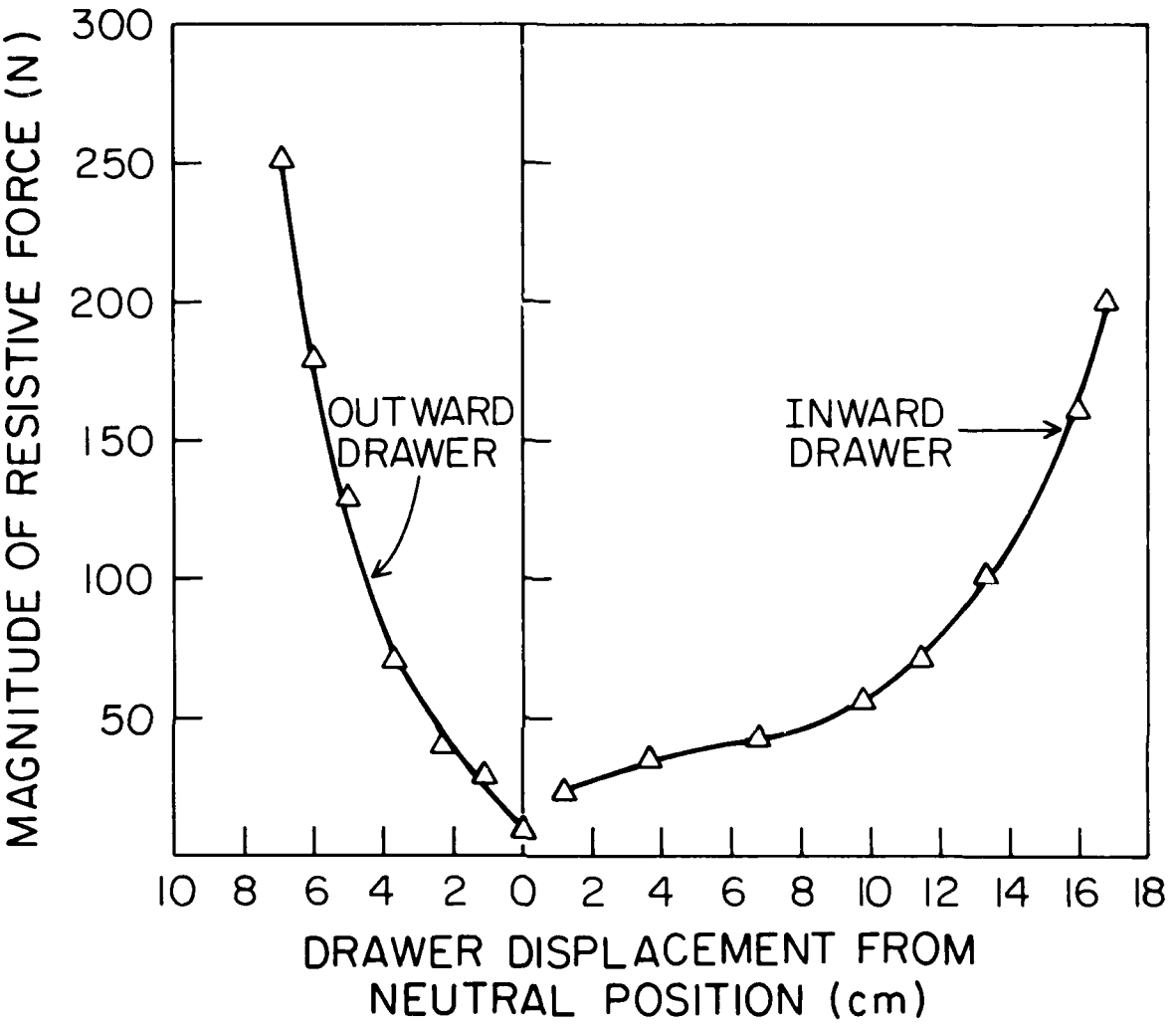

Fig. 14. Passive resistive force versus drawer displacement of the shoulder complex of the third subject for the $\theta = 90°$, $\phi = 30°$ upper arm orientation.

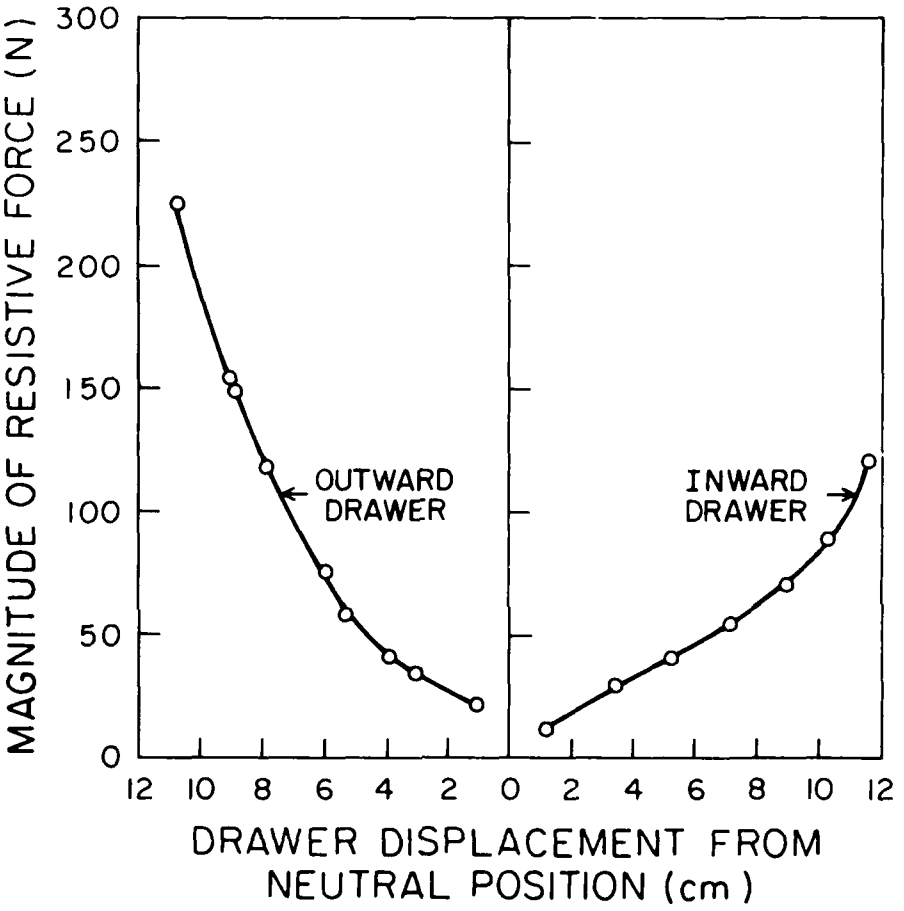

Fig. 15. Passive resistive force versus drawer displacement of the shoulder complex of the first subject for $\theta = 90°$, $\phi = 60°$ upper arm orientation.

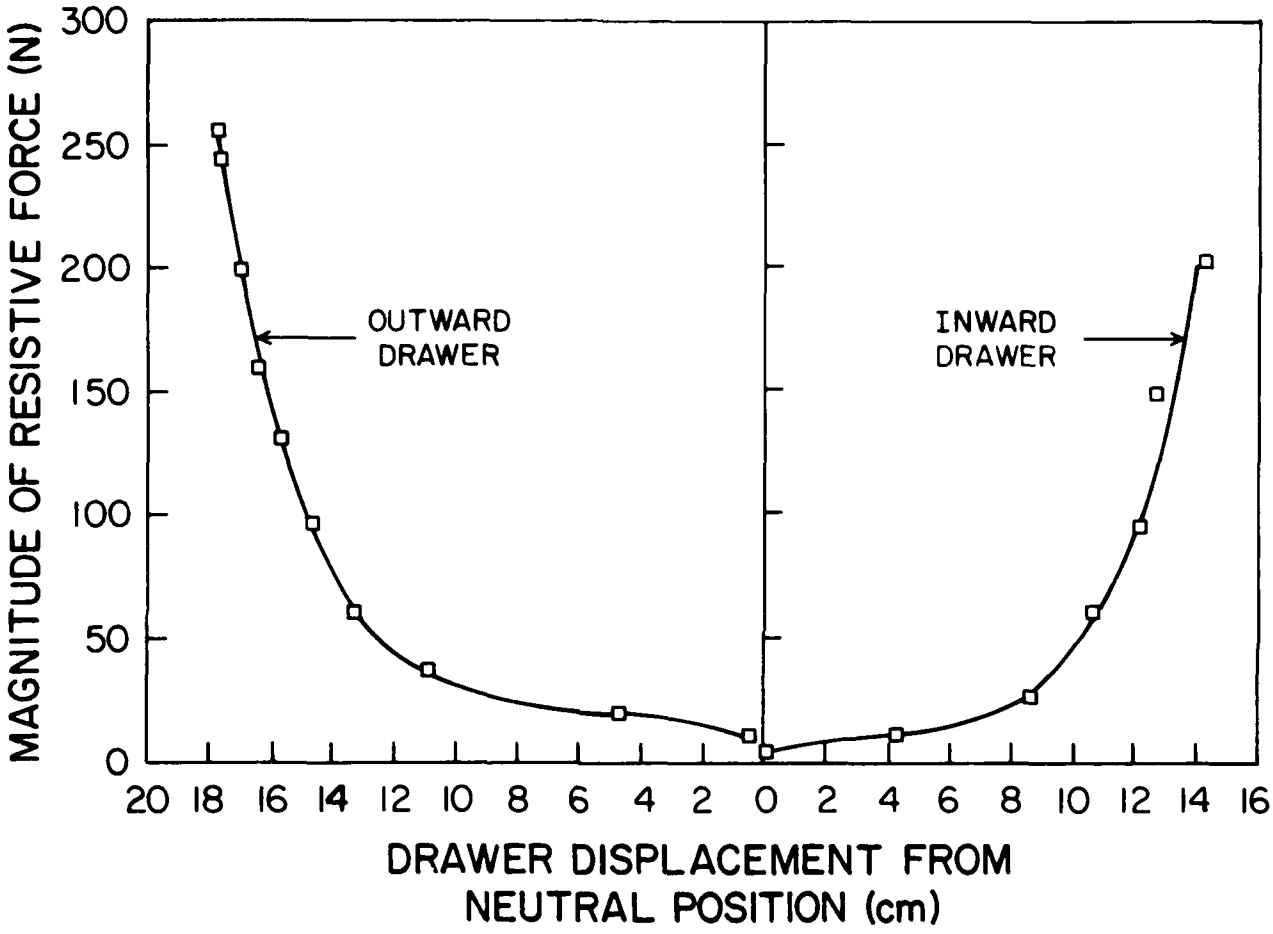

Fig. 16. Passive resistive force versus drawer displacement of the shoulder complex of the second subject for the $\theta = 90°$, $\phi = 60°$ upper arm orientation.

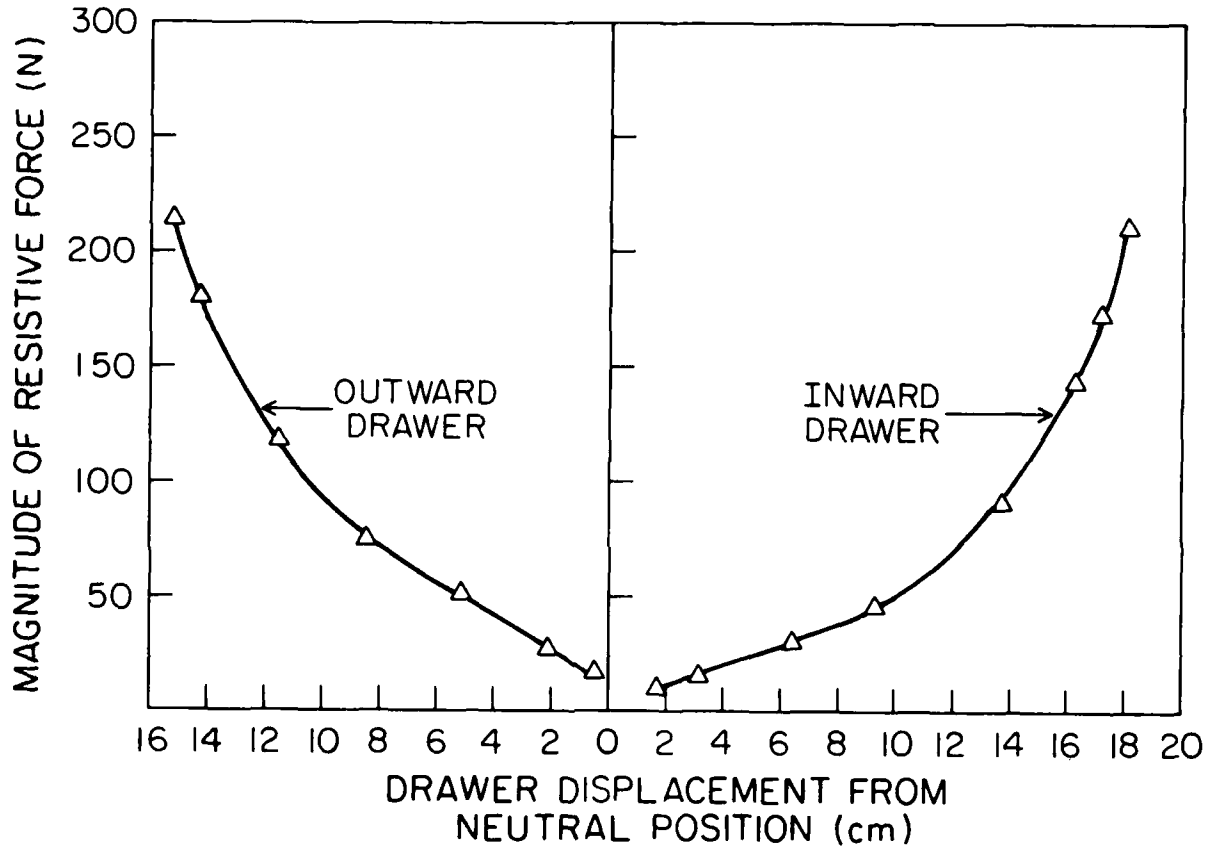

Fig. 17. Passive resistive force versus drawer displacement of the shoulder complex of the third subject for the $\theta = 90°$, $\phi = 60°$ upper arm orientation.

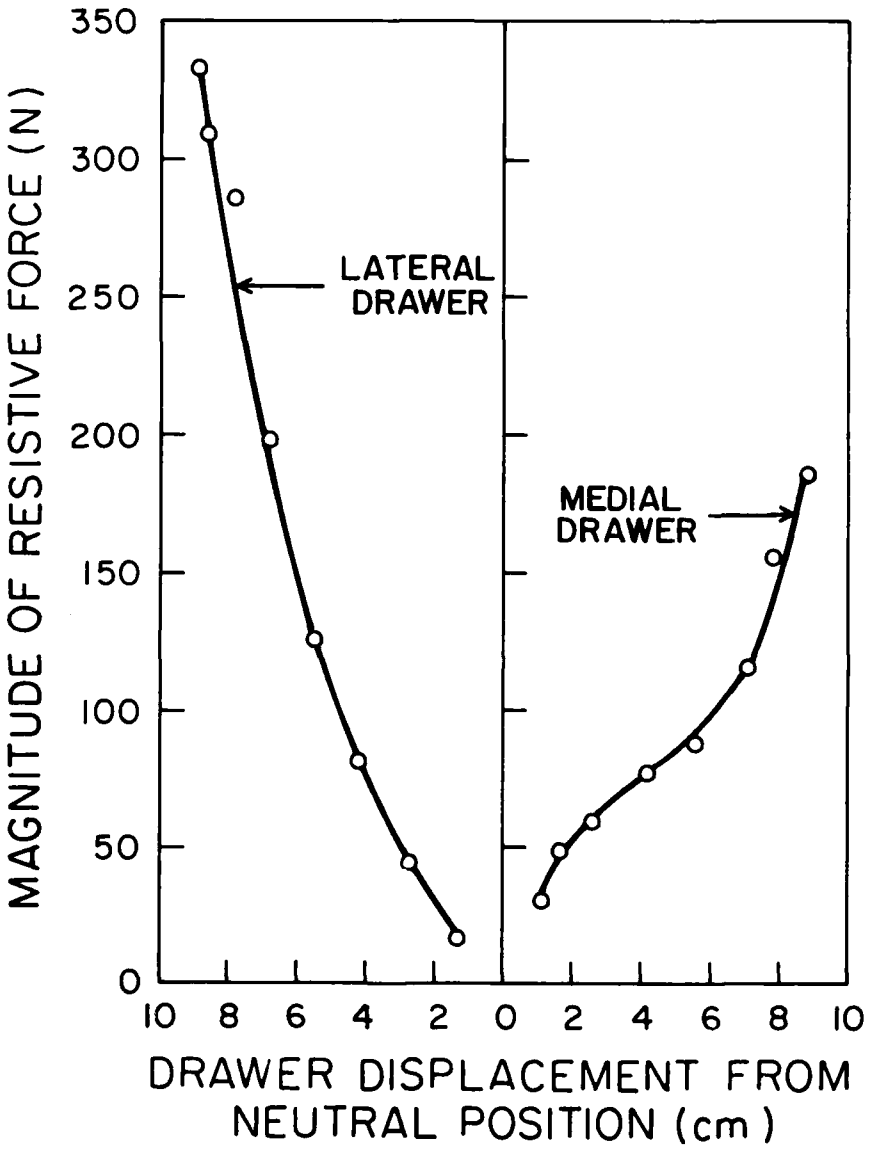

Fig. 18. Passive resistive force versus drawer displacement of the shoulder complex of the first subject for the $\theta = 90°$, $\phi = 90°$ upper arm orientation.

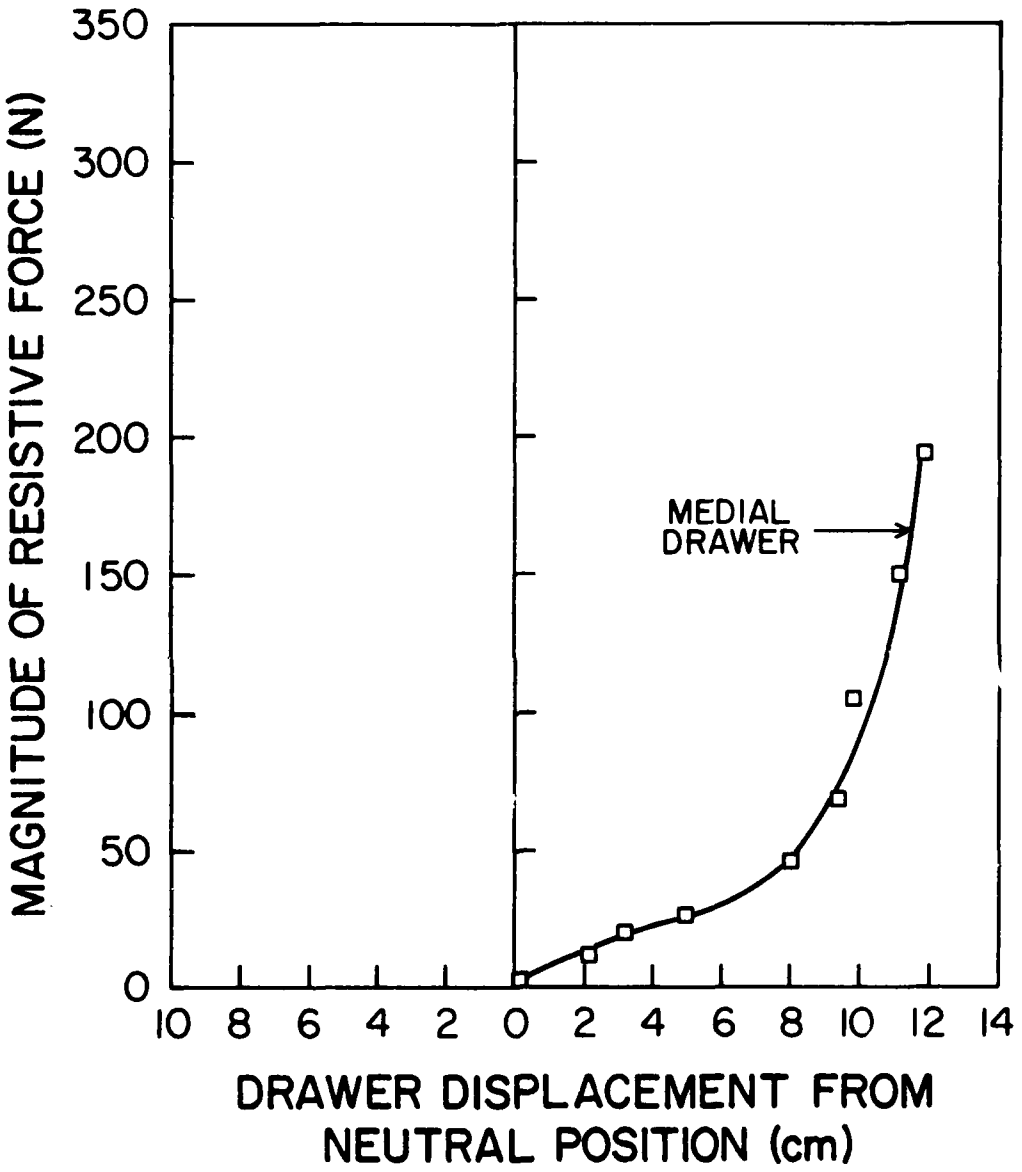

Fig. 19. Passive resistive force versus drawer displacement of the shoulder complex of the second subject for the $\theta = 90°$, $\phi = 90°$ upper arm orientation.

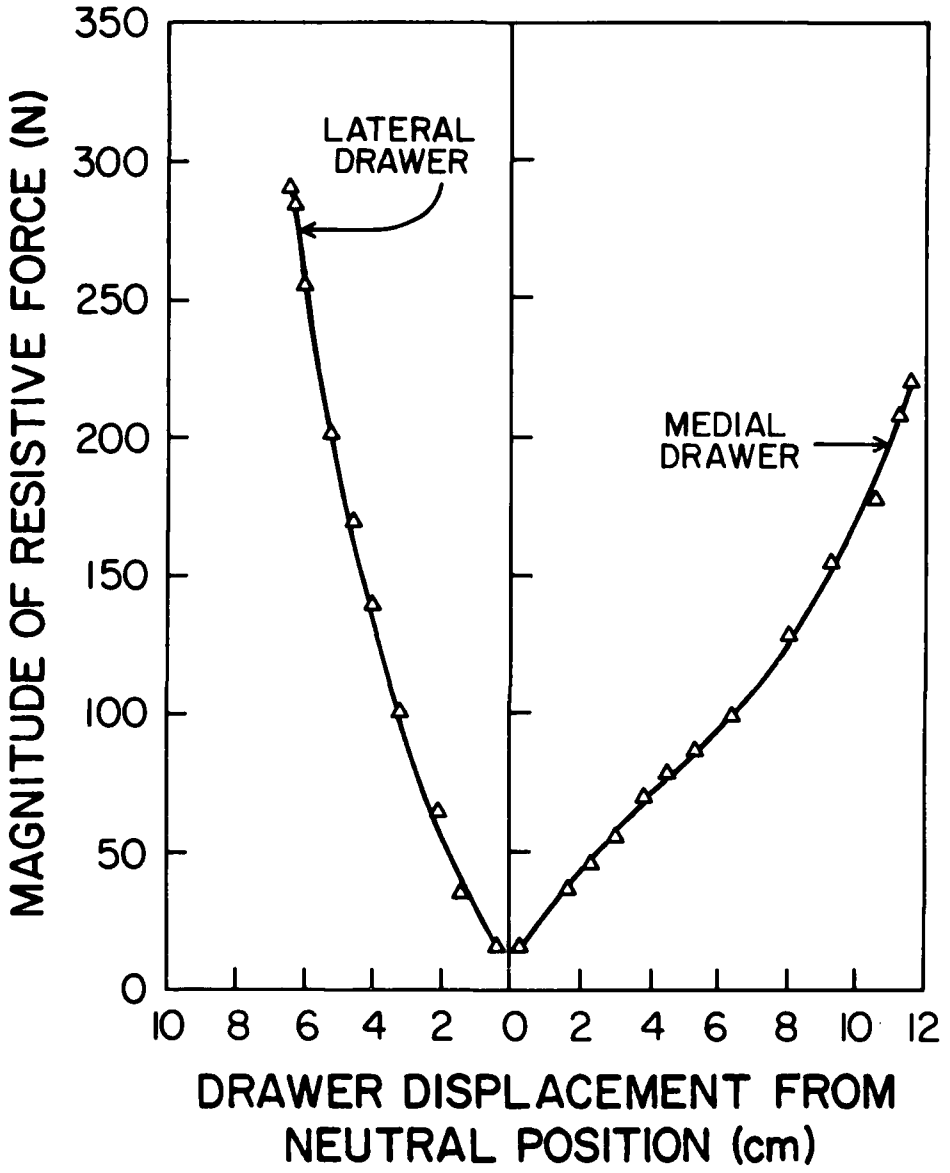

Fig. 20. Passive resistive force versus drawer displacement of the shoulder complex of the third subject for the $\theta = 90°$, $\phi = 90°$ upper arm orientation.

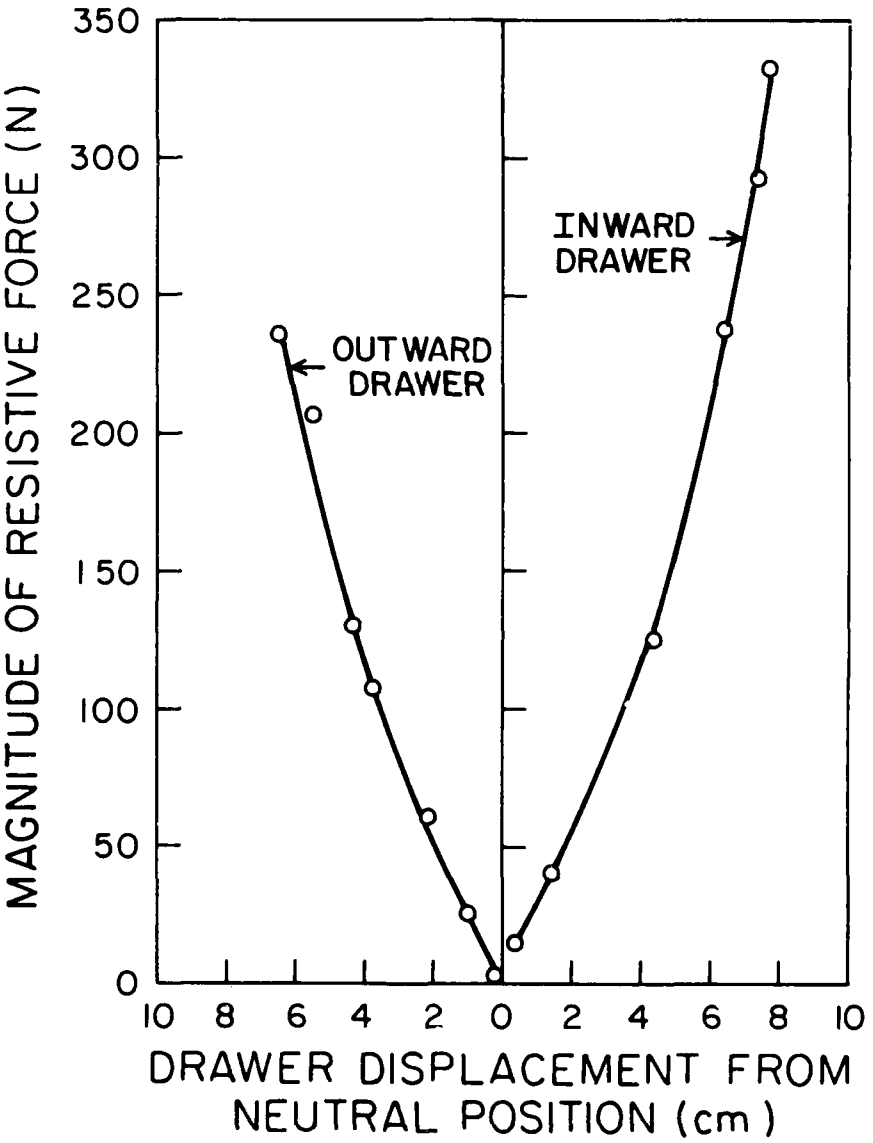

Fig. 21. Passive resistive force versus drawer displacement of the shoulder complex of the first subject for the $\theta = 90°$, $\phi = 115°$ upper arm orientation.

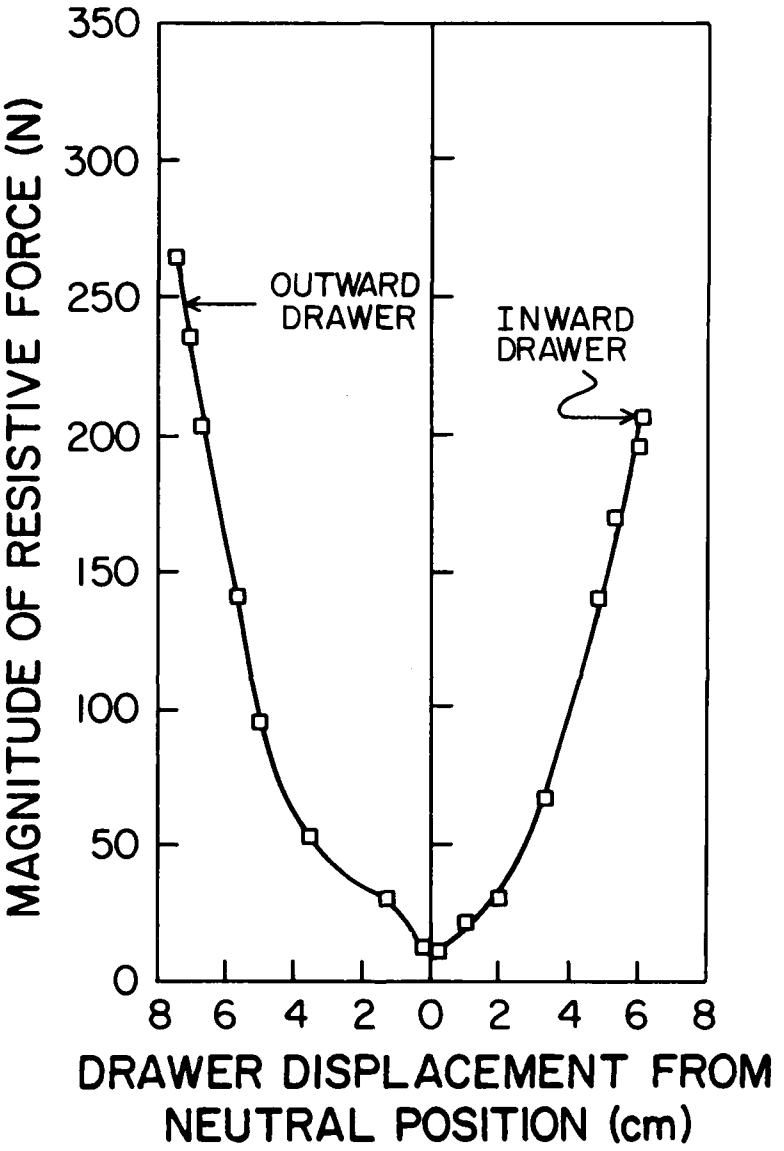

Fig. 22. Passive resistive force versus drawer displacement of the shoulder complex of the second subject for the $\theta = 90°$, $\phi = 115°$ upper arm orientation.

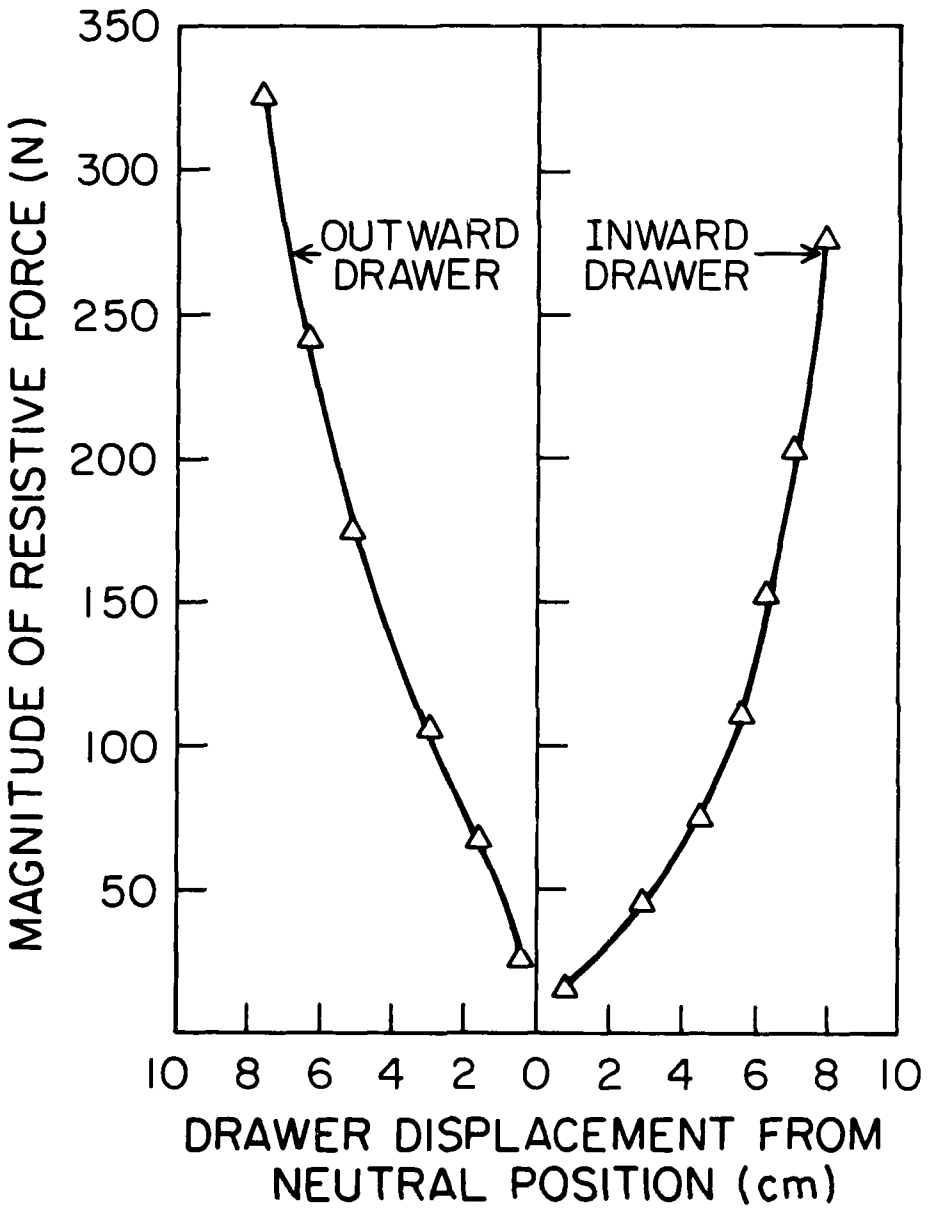

Fig. 23. Passive resistive force versus drawer displacement of the shoulder complex of the third subject for the $\theta = 90°$, $\phi = 115°$ upper arm orientation.

CONCLUDING REMARKS

The plots of the forced kinematic motion (drawer tests) of the shoulder complex presented in this report provide some quantitative results on the variability of the "axial stiffness" of the human shoulder complex dependent upon the upper arm orientation. Additional quantitative assessment of the axial stiffness of the shoulder complex can be made by curve fitting the numerical results plotted in Figs. 6-23. Two functions in the form of $y_1 = ae^{bx}$ and $y_2 = cx^d$ are chosen. Considering the fact that both exponential and power forms are the two functional representations which predominate in the elastic models for the constitutive stress-strain behavior of fibrous connective tissues, choice of these two functions is quite natural. The exponential form was originally proposed by Fung [19] and later used in various versions [20,21,28,29,30]; the usage of power form was equally wide-spread [22,23,25,26,27]. It is also important to point out that the axial stiffness characteristics of the shoulder complex are closely related to the constitutive behavior of the soft tissues associated with the shoulder complex.

Table II contains the coefficients, a, and, b, for the exponential curve. The numbers in parentheses in both Tables II and III designate the regression coefficients of determination, r^2, which indicate the degree of fit attained with the tabulated coefficients. Variation of the b coefficient for the exponential function with respect to upper arm orientation is shown in Fig. 24 for two subjects. The coefficients, c, and, d, for the power curve fitting are given in Table III. In certain cases the power curve appears to be the more appropriate choice. In the

curve fitting process for both types of functions the data points near the neutral position are excluded. In this region the curves exhibit a rapid increase initially, followed by a region of less rapid increase. It is believed that this phenomenon is an artifact of the testing procedure. It is possibly due to a reflex resistance caused by the activation of stretch receptors in the muscles of the shoulder complex.

Finally, although there are some intra-subject variations in the behavior of the axial stiffness of the shoulder complex for the subjects tested, strong similarities in the results do exist and, thus, certain characteristic response patterns for the axial stiffness of the human shoulder complex can be identified.

TABLE II

COEFFICIENTS, a and b, OF THE EXPONENTIAL CURVE, $y_1 = ae^{bx}$

UPPER ARM ORIENTATION & TYPE OF DRAWER TEST		SUBJECT 1		SUBJECT 2		SUBJECT 3	
		a	b	a	b	a	b
$\psi = 0^o$	SUPERIOR DRAWER	12.602 (0.999)	0.279	7.191 (0.999)	0.369	20.171 (0.972)	0.224
$\vartheta = 0^o$	INFERIOR DRAWER	8.248 (0.999)	0.331	6.538 (0.992)	0.353	11.179 (0.996)	0.280
$\varphi = 0^o$	ANTERIOR DRAWER	31.457 (0.987)	0.102	4.619 (0.993)	0.207	12.636 (0.998)	0.172
$\theta = 90^o$	POSTERIOR DRAWER	15.040 (0.991)	0.183	8.672 (0.993)	0.209	4.656 (0.997)	0.210
$\phi = 30^o$	OUTWARD DRAWER	4.008 (0.999)	0.259	3.763 (0.995)	0.264	20.754 (0.994)	0.152
$\theta = 90^o$	INWARD DRAWER	7.209 (0.999)	0.173	1.006 (0.971)	0.319	9.989 (0.998)	0.166
$\phi = 60^o$	OUTWARD DRAWER	16.855 (0.998)	0.241	3.602 (0.969)	0.227	16.386 (0.999)	0.403
$\theta = 90^o$	INWARD DRAWER	15.614 (0.997)	0.178	1.253 (0.998)	0.364	19.469 (0.972)	0.133
$\phi = 90^o$	LATERAL DRAWER	20.159 (0.994)	0.321	-		27.593 (0.993)	0.365
$\theta = 90^o$	MEDIAL DRAWER	34.313 (0.967)	0.185	5.075 (0.978)	0.305	39.015 (0.999)	0.150
$\phi = 115^o$	OUTWARD DRAWER	26.588 (0.988)	0.347	12.092 (0.996)	0.410	40.437 (0.985)	0.285
$\theta = 90^o$	INWARD DRAWER	29.963 (0.993)	0.340	15.508 (0.988)	0.452	16.360 (0.999)	0.328

TABLE III

COEFFICIENTS, c and d, OF THE POWER CURVE, $y_2=cx^d$

UPPER ARM ORIENTATION & TYPE OF DRAWER TEST		SUBJECT 1		SUBJECT 2		SUBJECT 3	
		c	d	c	d	c	d
$\phi = 0^o$	SUPERIOR DRAWER	1.707 (0.992)	2.071	2.230 (0.991)	1.939	4.334 (0.999)	1.659
$\theta = 0^o$	INFERIOR DRAWER	0.554 (0.983)	2.617	1.092 (0.971)	2.268	1.505 (0.980)	2.121
$\phi = 0^o$	ANTERIOR DRAWER	12.015 (0.920)	0.949	0.137 (0.961)	2.470	3.002 (0.941)	1.477
$\theta = 90^o$	POSTERIOR DRAWER	1.437 (0.999)	1.849	1.340 (0.970)	1.766	0.105 (0.973)	2.601
$\phi = 30^o$	OUTWARD DRAWER	0.120 (0.984)	2.699	0.118 (0.967)	2.698	6.407 (0.967)	1.231
$\theta = 90^o$	INWARD DRAWER	0.359 (0.983)	2.102	0.003 (0.948)	3.866	0.218 (0.990)	2.347
$\phi = 60^o$	OUTWARD DRAWER	12.920 (0.939)	1.083	0.090 (0.925)	2.633	18.723 (0.952)	1.242
$\theta = 90^o$	INWARD DRAWER	8.038 (0.970)	1.074	0.007 (0.990)	3.854	0.766 (0.970)	1.954
$\phi = 90^o$	LATERAL DRAWER	7.339 (0.996)	1.709	-		21.446 (0.991)	1.314
$\theta = 90^o$	MEDIAL DRAWER	16.080 (0.928)	1.071	0.551 (0.936)	2.309	15.461 (0.977)	1.048
$\phi = 115^o$	OUTWARD DRAWER	20.780 (0.998)	1.244	3.325 (0.991)	2.126	27.260 (0.991)	1.188
$\theta = 90^o$	INWARD DRAWER	29.043 (0.986)	1.136	8.121 (0.999)	1.825	5.397 (0.984)	1.771

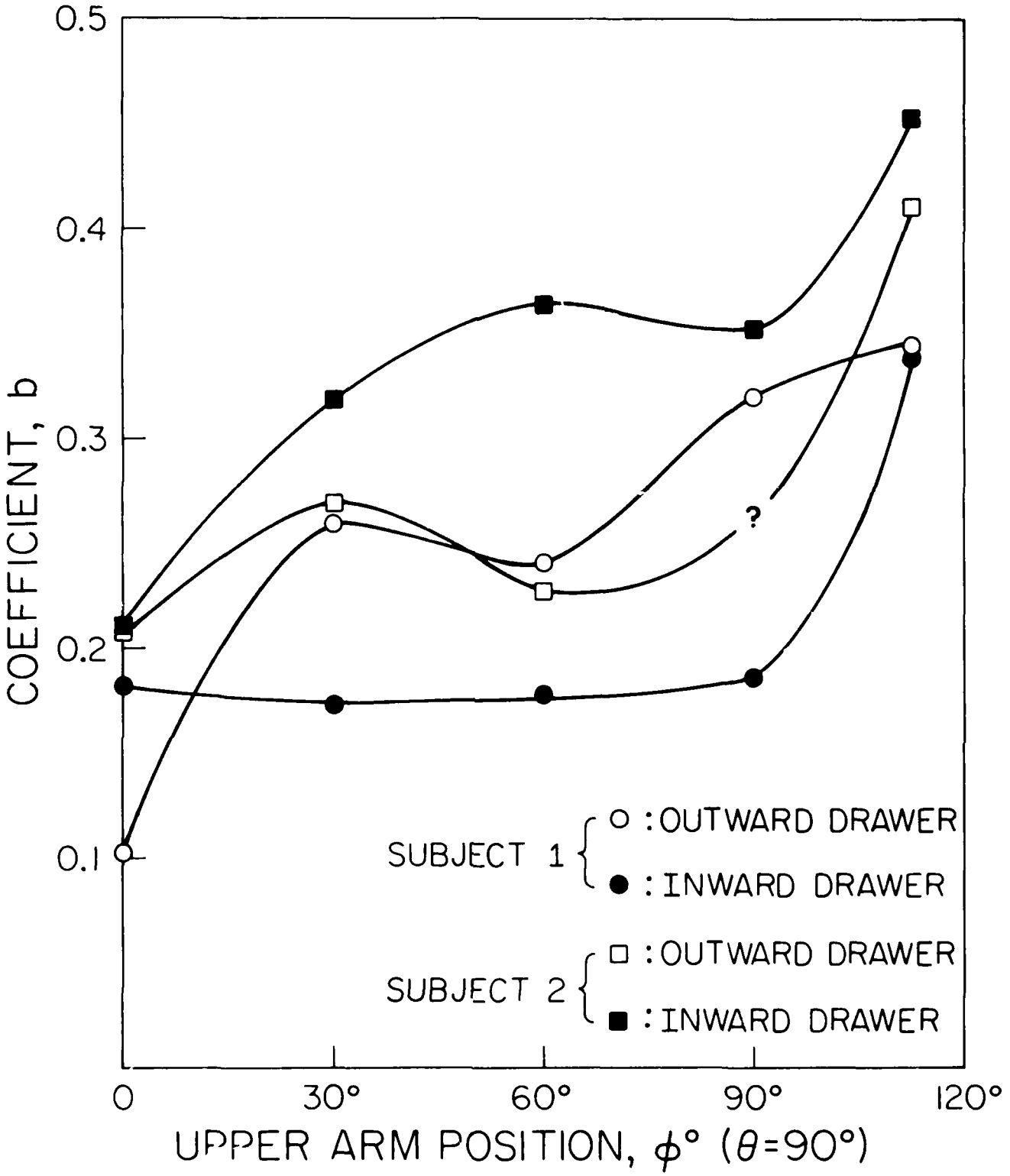

Fig. 24. The coefficients, b, of the exponential curve fitting of the passive resistance data of the shoulder complex at various upper arm positions (For the location indicated by ? data are not available).

REFERENCES

1. Engin, A.E., "Measurement of Resistive Torques in Major Human Joints," AMRL Report, No. AMRL-TR-79-4, 1979.

2. Engin, A.E. and M.H. Moeinzadeh, "Modeling of Human Joint Structures," AMRL Report, No. AMRL-TR-81-117, 1981.

3. Engin, A.E., "Long Bone and Joint Response to Mechanical Loading," AFOSR Report for the Contract No. F49620-79-C-0110, 1981.

4. Engin, A.E., "Passive Resistive Torques About Long Bone Axes of Major Human Joints," Aviation, Space, and Environmental Medicine, Vol. 50, No. 10, pp. 1052-1057, 1979.

5. Engin, A.E., I. Kaleps, R.D. Peindl, and M.H. Moeinzadeh, "Passive Resistive Force and Moments in Human Shoulder," Proceedings of the 32nd ACEMB, Vol. 21, p. 25, 1979.

6. Engin, A.E., "On the Biomechanics of Major Articulating Human Joints," an INVITED CHAPTER in NATO ASI-Progress in Biomechanics, edited by N. Akkas, Sijthoff & Noordhoff Publishers, Netherlands, pp. 157-188, 1979.

7. Engin, A.E. and I. Kaleps, "Active Muscle Torques About Long-Bone Axes of Major Human Joints," Aviation, Space and Environmental Medicine, Vol. 51, No. 6, pp. 551-555, 1980.

8. Engin, A.E., "On the Biomechanics of the Shoulder Complex," Journal of Biomechanics, Vol. 13, No. 7, pp. 575-590, 1980.

9. Engin, A.E. and R.D. Peindl, "Two Devices Developed for Kinematic and Force Data Collection in Biomechanics--Application to Human Shoulder Complex," Developments in Theoretical and Applied Mechanics, edited by J.E. Stoneking, Vol. 10, pp. 33-50, The University of Tennessee Press, 1980.

10. Engin, A.E., N. Akkas, and I. Kaleps, "Passive Resistive Force and Moments in Human Elbow Joint," 1980 Advances in Bioengineering, ASME Publication, pp. 229-232, 1980.

11. Engin, A.E., "Resistive Force and Moments in Major Human Joints," an INVITED LECTURE in Proceedings of the Eighth Canadian Congress of Applied Mechanics, pp. 181-200, 1981.

12. Engin, A.E., and M.H. Moeinzadeh, "Dynamic Modeling of Human Articulating Joints," Proceedings of the Third International Conference on Mathematical Modeling, University of Southern California, Los Angeles, California, p. 58, 1981.

13. Engin, A.E., and L. Kazarian, "Active Muscle Force and Moment Response of the Human Arm and Shoulder," Aviation, Space and Environmental Medicine, Vol. 52, pp. 523-530, 1981.

14. Moeinzadeh, M.H., A.E. Engin, and N. Akkas, "Two-Dimensional Dynamic Modeling of Human Knee Joint," Proceedings of the Fifth Annual Meeting of the American Society of Biomechanics, Case Western Reserve University, Cleveland, Ohio, 1981. (J. of Biomechanics, Vol. 15, No. 4, p. 346, 1982).

15. Engin, A.E., "Response of Human Shoulder to External Forces," Proceedings of the VIIIth International Congress of Biomechanics, Nagoya, Japan, p. 189, 1981.

16. Engin, A.E., and M.H. Moeinzadeh, "Two-Dimensional Dynamic Modeling of Human Joints." Developments in Theoretical and Applied Mechanics, edited by T.J. Chung and G.R. Karr, Vol. 11, pp. 287-296, 1982.

17. Engin, A.E., "Active Muscle Force Response of the Human Lower Limb," Aviation, Space and Environmental Medicine, Vol. 54 (1), pp. 52-57, 1983.

18. Engin, A.E. and M.H. Moeinzadeh, "Dynamic Modeling of Human Articulating Joints" to be published in International Journal of Mathematical Modeling, 1983.

19. Fung, Y.C., "Elasticity of Soft Tissues in Simple Elongation," American Journal of Physiology, Vol. 213, pp. 1532-1544, 1967.

20. Fung, Y.C., "Biorheology of Soft Tissues," Biorheology, Vol. 10, pp. 129-144, 1973.

21. Gou, P.F., "Strain-Energy Functions for Biological Tissues," Journal of Biomechanics, Vol. 3, pp. 547-550, 1970.

22. Haut, R.C. and R.W. Little, "Rheological Properties of Canine Anterior Cruciate Ligaments," Journal of Biomechanics, Vol. 2, pp. 289-298, 1969.

23. Hildebrandt, J., H. Fukaya, and C.J. Martin, "Simple Uniaxial and Uniform Biaxial Deformation of nearly Isotropic Incompressible Tissue," Biophysics Journal, Vol. 9, pp. 781-791, 1969.

24. Kaleps, I., "Characterization of Constraints and Forces Acting between Loosely Coupled Bodies with Application to Human Joint Mechanics," Ph.D. Dissertation, The Ohio State University, Columbus, Ohio, 1981.

25. Kenedi, R.H., T. Gibson, and C.H. Daly, "Bioengineering Studies of the Skin II," in Biomechanics and Related Bio-Engineering Topics, edited by Kenedi, R.M., pp. 147-158, Pergamon Press, Oxford, 1965.

26. Peng, S.T.J., R.F. Landel, and G.S. Brody, "In-vivo Study of Human Skin Rheology," Proceedings of the 6th M.E. Bioengineering Conference, pp. 350-354, Pergamon Press, Oxford, 1978.

27. Ridge, M.D. and V. Wright, "A Rheological Study of Skin," in Biomechanics and Related Bio-Engineering Topics, edited by Kenedi, R.M., pp. 165-175, Pergamon Press, Oxford, 1965.

28. Snyder, R.W. and L.H.M. Lee, "Experimental Study of Biological Tissue Subjected to Pure Shear," Journal of Biomechanics, Vol. 8, pp. 415-419, 1975.

29. Tong, P. and Y.C. Fung, "The Stress-Strain Relationship for the Skin," Journal of Biomechanics, Vol. 9, pp. 649-657, 1976.

30. Veronda, D.R. and R.A. Westmann, "Mechanical Characterization of Skin-Finite Deformations," Journal of Biomechanics, Vol. 3, pp. 111-124, 1970.

☆U.S. GPO: 1981-659 005/211


FILM
1-8